fibers

MDPI

Review

Analysis of the Passive Stabilization Methods of Optical Frequency Comb in Ultrashort-Pulse Erbium-Doped Fiber Lasers

Stanislav G. Sazonkin *, Ilya O. Orekhov, Dmitriy A. Dvoretskiy, Uliana S. Lazdovskaia, Almikdad Ismaeel, Lev K. Denisov and Valeriy E. Karasik

Scientific and Educational Center "Photonics and IR Technology", Bauman Moscow State Technical University, 105005 Moscow, Russia

* Correspondence: sazstas@gmail.com

Abstract: In this review paper, we describe the current state of the art to stabilize the output radiation of ultrashort-pulse (USP) fiber lasers and analyze passive methods to reduce the magnitude of fluctuations in the amplitude–frequency noise of output radiation. Regarding main noise characterization in mode-locked fiber lasers, we further consider the influence on laser operation of primary generation regimes starting up in cavities, such as solitons, stretched pulses, similaritons, and dissipative solitons. Then, we proceed to analyze the external and internal factors that affect the stability of the output radiation characteristics depending on the mode-locking mechanism and the resonator scheme.

Keywords: ultrashort-pulse fiber laser; mode-locking; stabilization of repetition frequency; stabilization of pulse duration; erbium fiber laser; fiber laser

Citation: Sazonkin, S.G.; Orekhov, I.O.; Dvoretskiy, D.A.; Lazdovskaia, U.S.; Ismaeel, A.; Denisov, L.K.; Karasik, V.E. Analysis of the Passive Stabilization Methods of Optical Frequency Comb in Ultrashort-Pulse Erbium-Doped Fiber Lasers. *Fibers* **2022**, *10*, 88. https://doi.org/10.3390/fib10100088

Academic Editor: Elena Anashkina

Received: 29 July 2022
Accepted: 28 September 2022
Published: 14 October 2022

1. Introduction

Over the past decade, there has been an increase in demand for highly stable laser systems of ultrashort pulses (USPs) in the frequency metrology field as frequency dividers, in telecommunications for synchronization and calibration of transmission systems, in astrophysics, in precision spectroscopy systems, in study of ultrafast processes, among others [1–5]. However, stabilizing laser systems with mode-locking has existed for about thirty years, and the creation of such highly stable systems is still a non-trivial task due to the complex nonlinear dynamics of USPs in a laser cavity. The first fundamental research in noise theory was carried out in 1963 under the leadership of McCummber [6]. The intensity fluctuations expected at the output of four-level continuous laser generators are calculated using linearized velocity equations. Further developments of the theory of noise, already for mode-locked lasers, were made by Haus and Mecozzi [7]. They pioneered the theory of mode-locked lasers, which applies to systems with additive pulse mode-locking and a Kerr lens. Using a linearized perturbation equation, they derived equations for pulse energy, carrier linewidth, frequency pulling, and timing jitter. In addition, they determined the influence of gain fluctuations and refractive index fluctuations. Additionally, worth noting, R. Paschotta made an enormous contribution to the study of mode-locked laser noise [8]. He developed a numerical model to calculate the noise of active and passively mode-locked lasers. His model was based on a pulse propagation algorithm with quantum noise sources, which allows studying a much broader class of phenomena than those available using analytical methods.

The next stage in the development of solid-state USP lasers is fiber lasers with ultrashort pulses. The use of optical fiber as an active medium has a number of significant advantages over solid-state lasers. The first important advantage is high reliability and compactness. Fiber lasers are characterized by all-fiber resonator circuits, or circuits in which the use of bulk optical elements (lenses, prisms, mirrors, etc.) is minimized, which makes it possible to reduce the number of alignment units and increase the reliability of the laser under vibration conditions. Additionally, it allows the use to place all the elements of the laser in a compact and ergonomic cases. In fiber lasers, it is relatively easy to arrange the cooling of the active element and temperature stabilization, since the ratio of area to volume of the resonator is of great importance. The second advantage is the simplicity and ease of use of fiber lasers, which are ensured by delivering a good quality laser beam through an optical fiber without the use of collimating systems, which reduce the reliability and energy performance of the radiation. Thirdly, fiber lasers have a high efficiency due to the almost complete absorption of pump diode radiation and efficient conversion of energy. For this reason, in our work, we focus on the study of USP fiber lasers. However, many of the principles and relationships in this article are also true for solid-state laser cavities on crystals.

Currently, navigation systems and global positioning systems (GLONASS, GPS, etc.) are developing rapidly. One of the promising ways to create such equipment is the development of an optical frequency standard based on highly stable laser sources of continuous radiation [9]. The most important task of using the optical frequency standard in global positioning systems is the frequency divider necessary to convert the optical frequency of a highly stable source to the radio frequency spectral band used by the onboard electronic component base [10]. One of the stages in the design of such a device is associated with the development of femtosecond lasers, which is a source of continuous equidistant narrow spectral lines with intervals between them equal to the pulse repetition frequency. At the same time, the full width of the spectrum is determined by the duration of one femtosecond pulse [11]. In other words, a femtosecond laser is a comb generator of high-monochromatic optical frequencies. If any component of the comb generator is associated with the optical frequency standard, then the position of any other spectral component is uniquely determined. One of the criteria for unambiguous determination of all frequencies of the generated comb is the exact determination of the pulse repetition rate of a femtosecond laser, which should be in the range from 50 to 100 MHz. Such a pulse repetition rate makes it possible to link the optical frequency standard with the frequencies at which the electronic equipment operates with high accuracy. To date, USP fiber lasers are capable of generating stable pulses with a duration of less than 100 fs and can be used to implement a stable frequency divider.

The optical frequency range can be used not only in global positioning systems, but also in many other scientific fields, such as spectroscopy, in particular, in terahertz-pulsed spectroscopy, which is an effective method for studying the parameters of materials transparent to THz radiation. For example, it is possible to study the dielectric permittivity of the medium or the refractive index in the THz range of the spectrum, which is important in medical applications for the non-invasive diagnosis of human diseases. This method makes it possible to determine various parameters of materials and, in particular, to study their structure by solving the inverse problem. However, the accuracy of the solution strongly depends on a significant number of factors, including the stability of the generation mode of USPs that excite THz radiation. As it was shown in the work [12], by numerical analysis, the accuracy of determining the refractive index of a substance does not exceed 5% for the instability of the duration of USPs at the level of several femtoseconds. It should be noted that the influence of pulse duration instability cannot be eliminated by any known signal filtering technique and, thus, a study of highly stable modes of femtosecond laser generation is required for accurate measurements of material parameters in the THz range of the spectrum.

However, the greatest success has been achieved in the field of spectroscopy, where a frequency comb is used for direct examination of the sample. It has been shown that a regular sequence of picosecond laser pulses with mode synchronization can be used for spectroscopy of the two-photon excitation of simple atoms with the same efficiency as a continuous laser with the same average power [13,14]. Although the narrow spectral range at the output of the picosecond laser did not allow for absolute binding, the role of the carrier offset frequency relative to the envelope in the equidistant frequency spectrum was already understood [15]. In the 2000s, after the first results on the study of the spectra of samples by means of a frequency comb generated by femtosecond laser sources, comb spectroscopy began to attract the interest of research groups [16].

Obtaining stable radiation parameters of USP lasers is a non-trivial task. The stability of the output parameters of the USPs is influenced by the stability of the cavity length, the cavity dispersion, the generation mode used, and other factors [4]. There are both passive and active methods for stabilizing the amplitude and time characteristics of the output radiation of USP fiber lasers. Active stabilization methods use systems with feedback, which makes it possible to achieve better output parameters compared to passive methods [10]. However, the use of feedback systems significantly complicates the implementation of such sources of laser radiation. Passive stabilization methods include methods associated with isolating the resonator from the influence of the external environment, and in particular, using thermal stabilization and vibration protection systems. Additionally, these methods of stabilization include the formation of USP generation modes in the laser cavity, which are less affected by noise factors.

Based on the earlier studies, the main types of fluctuations affecting fiber laser generators operating in the mode-locking regime are intensity noise, time jitter, and frequency comb noise. In this review article, we describe the current state of affairs in the field of stabilization of USP fiber lasers, and provide an analysis of the methods used to reduce the magnitude of fluctuations in the amplitude–frequency characteristics of laser radiation.

2. Noise Characterization in Mode-Locked Fiber Lasers

2.1. Intensity Noise of Mode-Locked Fiber Lasers

The intensity noise of mode-locked fiber lasers is systematically characterized for all main regimes of mode-locking over a wide range of parameters. Noise intensities are fluctuations in the average power of the pulses over a certain period of measurement time and characterize the average stability of the power. The intensity noise in the USP lasers, as well as for any other sources of laser radiation, is quantitatively determined through the relative intensity noise (RIN) level by the formula:

$$\mathrm{RIN} = \langle \Delta P(t)^2 \rangle_T \Big/ \langle P(t)^2 \rangle_T \tag{1}$$

where $\langle \Delta P(t)^2 \rangle_T$—rms optical power fluctuation; $\langle P(t)^2 \rangle_T$—average optical power of a pulse during the measurement time.

Intensity noise in USP lasers is caused both by quantum sources, such as amplified spontaneous emission (ASE) and vacuum noise [17], and external noise sources, such as, for example, the pump laser RIN, including noise source from the power supply. The response of the laser radiation intensity to disturbances is far from instantaneous. Any small perturbation causes a change in relaxation that will decrease in an exponential vibration considering the finite lifetime in the excited state in the amplifying medium. In the region of Fourier frequencies, at the resonance frequency of relaxation of oscillations, a change in the influence of perturbations on noise intensity is observed. If the oscillation frequency is higher than the relaxation frequency, the response to such oscillations decreases rapidly. This effect is similar to that of a low pass filter. The vibration relaxation frequency is usually in the region of several kilohertz for erbium and ytterbium USP fiber lasers. Noise caused by amplified spontaneous emission (ASE) and pump laser noise increases the laser's RIN to the vibration relaxation frequency. Since the pump noise level is usually much higher than the ASE noise level, pump noise dominates the RIN of the USP fiber lasers for frequencies below the vibration relaxation frequency. The RIN of the pump laser is almost wholly transferred to the USP fiber lasers at frequencies up to ≈15 kHz [18]. RIN of USP lasers at high frequencies approaches the quantum noise limit. Fluctuations of vacuum noise set the minimum noise level, the spectral power density of which is determined by the expression [19]:

$$S_{RIN}(f) = \frac{2h\nu_c}{P_{avg}} \tag{2}$$

where h—Planck's constant; ν_c—carrier center frequency; P_{avg}—average output power of USP lasers. For example, for USP lasers at a wavelength of 1550 nm with an average output power of 1 mW, the fluctuations of vacuum noise are limited to −156 dB/Hz, and for 10 mW and 100 mW—−166 dB/Hz and −176 dB/Hz, respectively. Consequently, the higher output power of the laser results in less noise.

Recently, achieving a reduction in RIN with fiber mode-locked lasers has become a very active research field, due to its relevance for various applications including vibrational imaging based on Raman scattering microscopy [20,21], photonic analog-to-digital converters [22,23], and gravitational wave detectors [24]. In the next subsection, we summarize the dependence of RIN on various conditions and parameters. In Table 1 shown summary of the state of the art of RIN measurements in mode-locked fiber lasers, with different types of mode-locking methods and stability increasing methods. To date, there is no theory with a full description of this dependence. Nevertheless, we expect this summary and discussion to be very helpful for understanding the behavior of the RIN and the ability to control it in mode-locked fiber lasers.

Table 1. Summary of the state of the art of RIN measurements in mode-locked fiber lasers, with different types of mode-locking methods and stability increasing methods.

#	Laser	RIN Values		Rms Rin Integration Range
		PSD at 10 kHz [dB/Hz]	Rms [%]	
1	78 MHz, NALM, Yb all-polarization-maintaining (PM) fiber laser (2020) [25]	−125	0.003	[1 Hz, 1 MHz]
2	78 MHz, NALM, Yb all-polarization-maintaining (PM) fiber laser (2020) [25]	−125	0.002	[10 Hz, 100 kHz]
3	700 MHz, NALM 215 fs, Yb:fiber laser (2018) [26]	−135	0.015	[10 Hz–10 MHz]
4	10-MHz, SESAM, all-normal dispersion all-PM Yb-fiber laser (2016) [27]	−117	0.018	[10 Hz–2.5 MHz]
5	32 MHz, 40 ps Yb fiber laser at 1032 nm (2019) [28]	−123	0.027	[1 HZ–100kHz]
6	60 kHz, SESAM, 1 ps Yb:glass fiber laser (2018) [29]	−125	0.023	[10 Hz–10 MHz]
7	161 MHz, NPE Yb-doped fiber laser, (2014) [30]	-	0.02	[1 kHz–5 MHz]
8	882 MHz, NPE Yb fiber laser, (2019) [31]	-	0.0074	[1 MHz–100 Hz]
9	54 MHz, 88 fs, NALM, Yb fiber laser (2021) [32]	−130	0.0055	[20 Hz, 1 MHz]
10	54 MHz, 88 fs, NALM, Yb fiber laser (2021) [32]	−145	0.02	[20 Hz, 10 MHz]
11	119 fs, all polarization maintaining (PM) Yb fiber laser based on NALM (2017) [33]	-	0.18	[1 Hz–1 MHz]
12	200 kHz, 22 fs pulse compressed of 460 fs Yb fiber laser at 1.03 µm (2020) [34]	−125	0.05	[2 HZ–100 kHz]
13	85 MHz, 50 fs, 0.16 nJ pulse energy based on NALM (2019) [35]	-	0.4	[1 Hz–1 MHz]
14	85 MHz, 50 fs,0.16 nJ pulse energy based on NALM, (self starting test and 0–45 °C high to low temperature test were carried out) (2019) [35]	-	0.07	[1 Hz–1 MHz]

The thermal stability of the active medium and resonator plays an important role in the issue of stability. As mentioned earlier, a transient relaxation oscillation within the active medium caused by any reason leads to an increase in the RIN amplitude. Thermal instabilities appear as the main cause of these relaxations, ensuring a stable thermal environment for the laser achieves a significant decrease in the value of rms-RIN. As we see in [34], there is a decrease in rms from 0.4% to 0.007% by setting the laser into a temperature chamber and running a long-term stability test (for 15 h). Additionally, low rms-RIN was achieved in [29] by implementing a temperature control (by thermoelectric cooler, which provides a constant temperature) on the active fiber. The rms-RIN increases with increasing temperature (0.023% at 11 °C, 0.027% at 12 °C and 0.030% at 13 °C).

The influence of pump power and optical power on RIN is one of the key factors affecting the stability of laser generation. To understand RIN more deeply, we took into consideration some operations in the measurement stage. Briefly, any photodetector used to measure the power spectral density of RIN (PSD-RIN) provides a current $I(t)$, with described PSD-RIN as [36]:

$$S_I(f) = S_e(f) + 2eI_{avg} + I_{avg}^2\, S_{RIN}(f) \tag{3}$$

The PSD divided by I_{avg}^2 provides the relative intensity noise:

$$RIN(f, I_{avg}) = \frac{S_e(f)}{I_{avg}^2} + \frac{2e}{I_{avg}} + S_{RIN}(f) \tag{4}$$

where $S_e(f)$ is the electronics PSD, e is a single electric charge, f is the frequency, I_{avg} is the average photocurrent that is proportional to optical power $I_{avg} = \frac{e\eta}{h\upsilon}p$, and $S_{RIN}(f)$ is the PSD of the classical fluctuation of the laser intensity. The three terms on the right-hand sides of Equation (3) are linked to three deferent noises, respectively, the electrical noise, which is due only to the photodetector; the laser shot noise (quantum noise); and the laser excess (classical) noise. Both the quantum and classical noises are inherent to the laser source. In other words, the measured power spectral density of RIN with a photodetector consists of electronic noise that is inversely proportional to the square of average current (therefore to the optical power), shot noise is inversely proportional to the average current (therefore to the optical power), and the excess noise that is independent of the optical power. Equation (5) explains why the RIN decreases when the optical power is increased [37]. It should be noted that electronic noise can be made negligible by choosing a high-quality photodetector and laser intensity.

On the other hand, the RIN (PSD and rms) decreases by increasing the pump power, a measurement of PSD-RIN in [38] with various pump powers (77–168 mW) showed a decrease in RIN by increasing pump power especially at a frequency below 1 kHz where the RIN of the mode-locked laser was higher than the RIN of the pump laser. Moreover, increasing the pump power leads to an increase in the cavity finesse, which determines the amplification factor per round trip. Higher cavity finesse leads to low RIN due to decreased cavity losses [39]. As shown in [40], RIN increases linearly with increasing cavity losses by decreasing the cavity finesse. However, there is a certain case of soliton laser [37] when increasing the pump power and the optical power led to high excess noise; therefore, with the same optical power, RIN decreased with pump power 370, 558, and 627 mW, respectively.

Total net-cavity dispersion β_2 has a direct effect on RIN and is related to the dispersion of its component elements and their lengths. Pulse-shaping mechanisms are taken into account when it comes to dispersion [41] because net-cavity dispersion plays a significant role in laser dynamics. The output pulse characteristics of an Er-doped fiber laser as a function of β_2 were determined in [42], and the results show that increasing β_2 from -0.04 ps^2 to $+0.04$ ps^2 changes the pulse shape from soliton to dissipative soliton through stretched pulse operation. Figure 1 shows the latest rms-RIN values with various total net-cavity dispersion. We can observe that the lowest RIN could be achieved with anomalous dispersion in [26,32,35], while in [30,43] with normal dispersion; otherwise, a low-RIN could be achieved when the intra-cavity dispersion was set to close to zero [25,34,44].

The PSD-RIN of Yb soliton fiber laser was measured in [37] with various total intra-cavity dispersion values (-3.7 , -10.6 ps^2, -37.5 ps^2), and the results showed a decrease in RIN as a function of optical power ($p > 10$ mW) only at $\beta_2 = -37.5$ ps^2, while a maintenance of RIN was seen for the other values of total intra-cavity dispersion. This can be explained as follows: with optical power $p > 10$ mW, excess noise dominates and the dependence of RIN on β_2 is stronger than its dependence on optical power. Experimentally, it was observed that the excess noise of the soliton regime decreases with increasing the net intra-cavity dispersion.

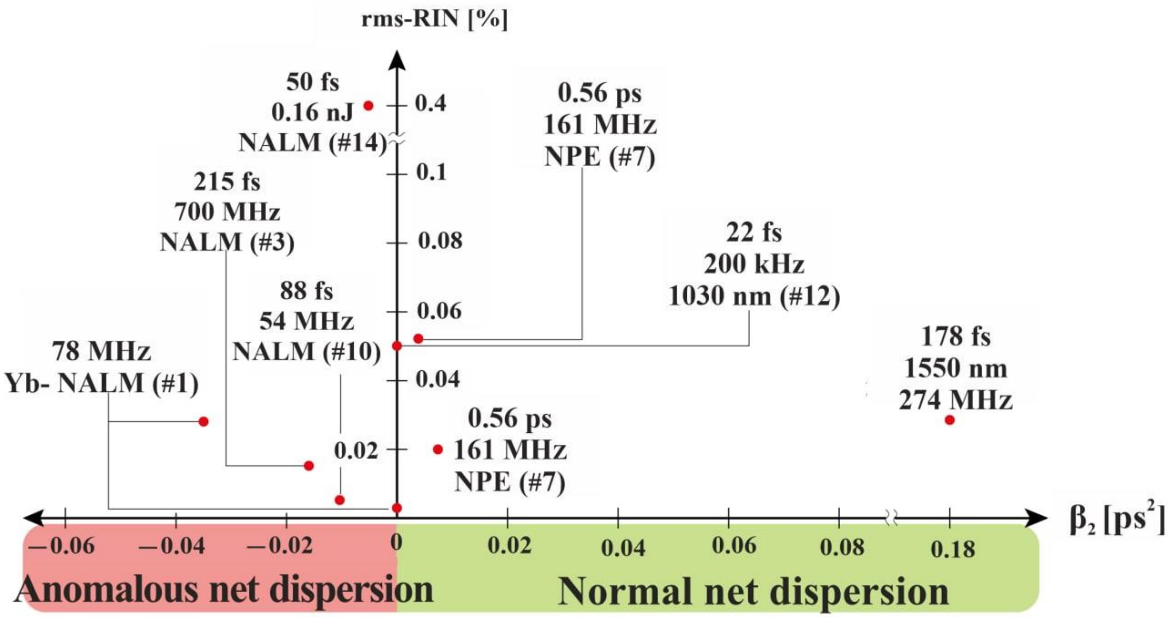

Figure 1. Summary of the rms-RIN performance of passively mode-locked fiber lasers with various net dispersion values.

The insertion of a narrow bandpass filter into a cavity of mode-locked fiber laser has an obvious effect on RIN, for example, a 7 nm bandwidth filter was used in Yb fiber mode-locked laser based on NPE with normal dispersion [30]. The rms-RIN was reduced from 0.37% to 0.02% with net dispersion $\beta_2 = 0.008$ ps^2 (with pulse duration $\tau = 0.16$ ps), and from 0.14% to 0.057% with net dispersion $\beta_2 = 0.004$ ps^2 ($\tau = 0.012$ps). Additionally, with an all-normal dispersion (ANDi) regime $\beta_2 = 0.02$ ps^2 ($\tau = 0.11$ ps), rms-RIN was reduced from 0.37% to 0.02%. After inserting the filter, the pulse duration was 0.11 ps for all the afore-mentioned regimes. The reduction in RIN by filtering has also been demonstrated in soliton [45] and soliton-similariton regimes [46].

The simulation of the saturation of active fiber was conducted in [47] to study the transfer function of RIN as a function of the seed power and the frequency. It led to influencing the saturation of active fibers on the amplitude noise. The behavior of this saturation is related to the effective lifetime of the excited state, which is expressed by:

$$\frac{1}{\tau_{eff}} = \frac{1}{\tau} + \frac{\Gamma \lambda_{laser}}{hcA} \sigma_{e_{laser}} P_{laser} \tag{5}$$

where τ is the natural life time of the excited state, Γ is the overlap of the signal light with the doped region, λ_{laser} is the wavelength of the signal light, h is Plank's constant, c the speed of light, A is the doped area, $\sigma_{e_{laser}}$ is the emission cross-section, and P_{laser} is the output power. To the best of our knowledge, there is no experimental research with the same aim as this systematic study; however, this result opens up the possibility of optimizing the noise characteristics, for example, the core diameter, which according to the simulation, influences the frequency range over which the input RIN of the signal is damped at the output.

By definition, RIN is a quantity that characterizes the stability of the laser radiation intensity. As shown in [4], the RIN value in USP fiber lasers is influenced by the generation mode and the pulse shaping mechanism, the total GVD of the cavity elements, and spectral filters in the cavity. The minimum value of RIN is observed when the total GVD of the resonator elements is zero. Spectral filters reduce laser intensity noise, increasing the pulse duration and decreasing the peak power [48].

2.2. Timing Jitter Characterization of Mode-Locked Fiber Lasers

Along with the instability of the laser output intensity, there is also temporal instability. Timing jitter is the main parameter characterizing the stability of the temporal characteristics of the laser output radiation. Jitter is the temporary deviation of the position of the pulse envelope from its ideal position, determined by the period of the pulse bypassing the resonator (for USP lasers with self-triggering, this temporary deviation is accidental since there is no mechanism for returning the pulse to the desired position). Additionally, jitters are rightly called the integral characteristic of the phase noise of all frequency components of the propagating pulse. It should be noted that the power spectral density of jitters and phase noise of the pulse repetition frequency (f_{rep}) and its harmonics (nf_{rep}) are identical, assuming the absence of phase noise during the optoelectronic signal conversion by the radiation receiver.

Time jitter is related to the phase noise of the spectral components of a pulse train. In the absence of technical noise, quantum noise limits the mode-locked laser jitter; however, in most cases, the jitter is determined by the vibration and drift of the laser cavity. The timing jitter of various mode-locked lasers can be very low—in some cases substantially less than high-quality electronic oscillators. It is especially true for small time scales when the laser can be used as a very accurate timing device (such as a metronome of sorts).

When calculating and studying jitters, special attention was paid to the works of G. Haus and R. Paschotta [7,8,49–51]. Note that these theories ignore laser power fluctuations due to pump laser noise and ignore low-frequency noise sources, such as temperature changes and acoustic vibrations, which can be compensated for by adjusting the cavity length. Jitters in fiber USP lasers can be divided into direct jitter and Gordon–Haus jitter [51]. Conventional jitters are caused by spontaneous emission amplification (the spontaneous emission amplification defines the fundamental jitter limit), while the Gordon–Haus jitter is due to the carrier's center frequency change through group velocity dispersion (GVD) fluctuations. In [52], an equation was obtained for evaluating jitters in fiber USP lasers:

$$J^2 = \frac{2h\nu}{E^2}(g-1)\left[\frac{4D_2^2}{T_R^2}\tau_g^2 C I_\omega + I_t\right]\frac{T}{T_R} \tag{6}$$

where E—pulse energy; T_R—time pulse passage the cavity; D_2—total GVD of the cavity; T—measurement time; $I_\omega = \int t^2 E(\omega) d\omega$—integral spectral density of pulse energy; $I_t = \int t^2 E(t) dt$—integral pulse energy over time; τ_g—time constant that takes into account the change in frequency due to the width of the laser medium gain band and equal: $\tau_g \approx (T_R/g)\left(\Delta\Omega_g/\Delta\Omega_p\right)^2$; $\Delta\Omega_g$ и $\Delta\Omega_p$—spectrum width at half maximum of active medium and pulse, respectively; C—pulse chirp factor. The first part of Formula 6 is the Gordon–Haus jitter, and the second is the jitter. As can be seen from the formula, the jitter is influenced by the pulse energy, the total GVD, and the time of the pulse round trip. Therefore, to reduce the jitter value, it is necessary to reduce the total GVD of the resonator elements to zero, maximize the pulse energy and increase the length of the resonator. The following sections discuss the jitter for each mode-locking regime.

Note that, in addition to ASE, acoustic noise and RIN have a significant impact on jitter. Acoustic noise is observed in the range from tens of hertz to 1 kHz [53]. An acoustic enclosure and acoustic shielding of a fiber laser can significantly reduce acoustic noise exposure. RIN can be associated with jitter in three ways [49]: phase change in the amplifying medium (Kramers–Kronig relations), spontaneous steepening of the pulse front, and slow bleaching absorber. Using a fast anti-reflective absorber does not affect jitter. Spectral filters in the resonator reduce the jitter value and RIN but increase the pulse duration [48].

2.3. Noises of Optical Frequency Comb in Mode-Locked Fiber Lasers

As is widely known, after the Fourier transform of the electromagnetic field of a mode-locked laser pulse train, a discrete comb spectrum can be obtained in the frequency domain. The representation of the output signal of a mode-locked laser in the time and frequency domain is shown in Figure 2. The deterministic behavior of the optical frequency comb spectrum is most succinctly described by the comb equation. The optical field of a sequence of laser pulses can be described by the carrier frequency $\nu_c = \omega_c/2\pi$, which is modulated by the periodic pulse envelope $A(t)$ [54]. In general, the generation process of a mode-locked laser is a sequence of pulses following at intervals of 1 to 10 ns. Due to the periodicity of the pulses, the optical field can also be described as a sequence of Lorentz lines:

$$\widetilde{A}(\nu) = \frac{|\widetilde{a}(v-\nu_c)|}{2\pi T_R^2} = \sum\nolimits_n \frac{2\Delta\nu_n}{(v-\nu_c)^2 + \Delta\nu_n{}^2} \tag{7}$$

where $\widetilde{a}(v)$ is the Fourier transform of the pulse envelope function $a(t)$, ν_n is the position of the line comb (no noise) at $\nu_n = f_{ceo} + n\cdot f_{rep}$, and $\Delta\nu_n$ is the line width of the line comb. Accordingly, the width of the comb line can be expressed as:

$$\nu_n = \Delta\nu_{\Delta\theta} + [2\pi\tau(v-\nu_c)]^2\Delta\nu_{\Delta T} \tag{8}$$

where $\Delta\nu_{\Delta\theta}$ and $\Delta\nu_{\Delta T}$—diffusion constants for $\Delta\theta$ and ΔT_R, respectively; and τ—pulse width. Thus, the fluctuation of the comb linewidth and the corresponding frequency noise can be expressed as a linear combination of diffusion constants for jitter and phase noise in the time domain. Obviously, the minimum comb line width is observed at the center frequency and increases towards the edges of the optical spectrum envelope due to the jitter contribution.

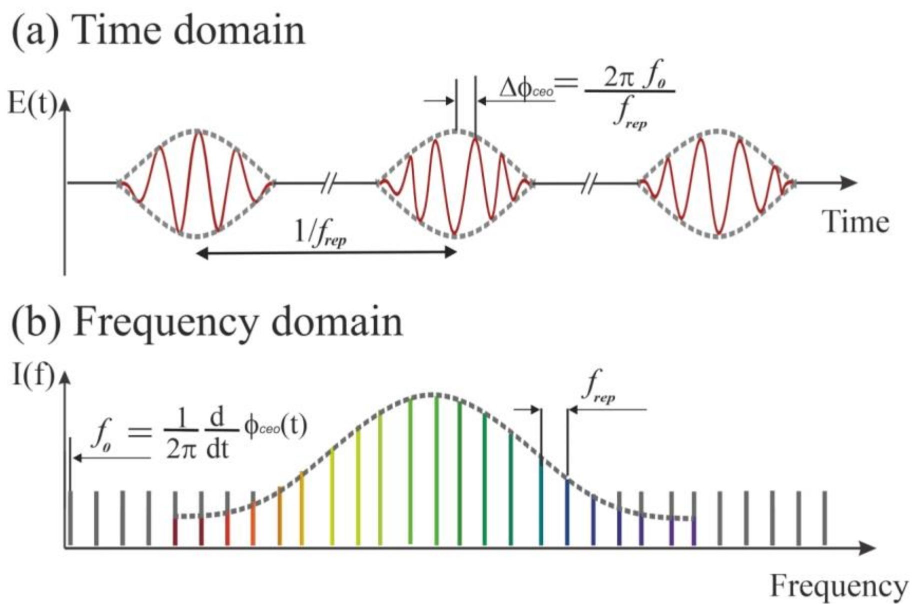

Figure 2. Time (**a**) and frequency (**b**) domain representation of a mode-locked laser output. The frequency comb of longitudinal modes corresponds to a train of short pulses spaced by the cavity round-trip time $t_{rt} = 1/f_{rep}$.

In a passive mode-locked laser, the saturable absorber provides a fixed phase relationship. The USP train results from beats (coherent superposition) of the phase-locked modes. Meanwhile, the same periodic modulation effect naturally correlates with any random fluctuations, such as ASE, pump noise, or jitter. Otherwise, the series of USPs will collapse to a continuum due to dephasing effects [4,55]. In this regard, the coherence of the comb teeth is limited only by the quality of the mode locking process.

The model that conveys the above phase locking mechanism is simply expressed as:

$$\nu_n(t) = f_{ceo}(t) + n\, f_{\,rep}(t) \tag{9}$$

where any perturbation violates only two degrees of freedom, namely the intermode interval and the offset frequency of the optical frequency comb. The integration of Equation (9) allows us to obtain a record of the dependence of the instantaneous phase of all signals [56]:

$$\varphi_n(t) = \varphi_{ceo}(t) + n\, \varphi_{\,rep}(t) + \phi_n \tag{10}$$

where $\varphi_n(t)$, $\varphi_{ceo}(t)$, and $\varphi_{\,rep}(t)$ are the instantaneous phase angles $\nu_n(t)$, $f_{ceo}(t)$, and $f_{\,rep}(t)$, respectively; and ϕ_n denotes the constant of integration. Obviously, Equation (10) maintains a fixed phase relationship between adjacent comb lines in the presence of noise. Certain perturbations will cause the comb to breathe around one fixed point frequency, ν_{fix}, where the effects $n_{fix} \cdot \varphi_{rep}(t)$ and $\varphi_{ceo}(t)$ are exactly canceled. Comb-line phase fluctuations will be leveraged in terms of the offset from the fixed point. In the following, we introduce the fixed points for various noise sources. Accordingly, the comb-line noise property is analyzed in terms of noise type [4].

In this regard, the frequency to phase noise ratio of each generation mode is an important parameter for assessing the quality of the frequency comb. Speaking about the noise of the frequency comb, one should distinguish directly between the fluctuations in the width of the spectral lines themselves that make up the comb and the noise of the envelope relative to the carrier, which means the fluctuation of the zero tooth of the generated frequency comb. Each of these types of noise can be caused by several reasons.

Speaking of fluctuations in the linewidth of the spectral lines of the frequency comb, two noise factors should be distinguished: the limit of the Schawlow–Towns linewidth and technical noise caused by instrumentation.

The Schawlow–Towns linewidth limit is an equation derived in 1958 and determines the fundamental limit of the width of the frequency lines generated by resonators [57]. In general, this formula is as follows:

$$\Delta v_{laser} = \frac{4\pi h\nu(\Delta v_c)^2}{P_{out}} \tag{11}$$

with the photon energy $h\nu$, the resonator bandwidth Δv_c (half width at half maximum (HWHM)), and the output power P_{out}.

In accordance with this formula, the width of the spectral line of a laser is fundamentally limited by the existence of spontaneous emission in the resonator. The line width limit expression is [58]:

$$S_f^{ASE}(f) = \frac{f_{rep}^2}{2\pi^2}\left(\frac{(1+n_{ASE})h\upsilon_0 G}{P_{cp}}\right) \tag{12}$$

where n_{sp}—amplified spontaneous emission coefficient; G—amplification inside the resonator; and P_{cp}—intracavity pulse power.

However, in practice, approaching the linewidth limit is unattainable, due to the presence of side technical noise in lasers. The reasons for the appearance of technical noise of frequency combs in mode-locked fiber lasers include, first of all, factors such as fluctuations in the cavity length due to temperature changes, and pump source noise.

However, for carrier and envelope phase noise, the situation is somewhat more complicated. The origin of noise is different in different frequency ranges. For frequencies below 1 kHz, this is mainly introduced by losses in the resonator; for the frequency range from 1 kHz to 100 kHz, it is mainly introduced by the pump noise; and for the frequency range above 100 kHz, it is mainly introduced by quantum noise generated by amplified spontaneous emission [39,59]. Let us consider in more detail the causes of phase fluctuations of the carrier frequency relative to the envelope, since this criterion is the most important for the frequency comb stabilizing. For today, laser generators emitting in the near infrared

(IR) range are capable of generating pulses with a duration of about 5 fs. Due to such a short duration, the field of such pulses can no longer be adequately described by its cycle-averaged intensity envelope. Instead, its actual shape depends on the phase between the carrier and its envelope, the Carrier Envelope Phase (CEP). Control over this parameter has long remained difficult to achieve, which becomes clear if we take into account the difficulty of measuring such small-time events. Because one light cycle of about 3 fs corresponds to a 2π phase, maintaining a constant carrier-to-envelope offset of $\pi/10$ (300 mrad) results in an accuracy of 150 as of temporal instability between the pulse envelope and the carrier wave—a value far beyond the picosecond temporal resolutions of modern electronics. A breakthrough idea arose in the field of timing or, more importantly, precision metrology, with the realization that the spectral properties of all laser radiation are determined by two easily measurable radio frequencies. This provided a direct link between radio and light frequencies, opening up an unprecedented level of accuracy in optical metrology [60]. The relationship between the characteristics of the frequency comb and the pulse-to-pulse phase evolution was realized early [15], and when the phase shift controls [61] were combined with the absolute frequency measurement [62], the phase shift was controlled.

To date, methods for measuring the CEP of a laser pulse with a duration of several cycles are well-developed based on a number of methods, such as f-2 interferometry [63], frequency-resolved optical grating using photoionization [64], dispersive Fourier transform [65], and angularly resolved photoelectron spectra of noble gas atoms in circularly polarized pulses with several cycles [66]. In addition to the aforementioned work, since 2009, much attention has been paid to the method for determining CEF by stereographic detection of high-order above-threshold ionization (ATI) spectra of noble gas atoms [67], which is also called stereo-ATI CEPmeter (CEPM) [68]. CEPM can be used to perform real-time CEP measurements for each individual pulse with high accuracy [67] for a laser system with a repetition rate up to 100 kHz [69], and high power, up to several terawatts [70]. If the measured CEP can be written to a computer along with the experimental data for each laser pulse, the experimental data dependent on the CEP can be extracted using offline analysis. This method, called phase marking [68], was used to study the effects of CEP for non-sequential [71] and sequential [72] double ionization and H_2 ionization and dissociation [73,74], as well as to develop the attosecond sweep method [75], and measurement of the refractive index dispersion [76], etc. Due to the strong dependence of the CEP of the high-order nonlinear processes involved, a high accuracy of the CEPM measurement can be achieved. The physical principle of CEPM is based on the radical CEP-dependent left-right skewness of high-order ATI outputs with angular resolution [77], and the CEP-dependence of this skewness can be an order of magnitude stronger than that of direct ATI [67].

In 2011, an accuracy of 113 mrad was reported [68] over the entire 2π range for a typical CEPM. In addition, it has been documented that a higher accuracy can be achieved with shorter pulse durations [78]. On the contrary, over a long time, the drift of the laser power (or intensity) will affect the accuracy of the CEPM [79], which can be eliminated by periodic recalibration.

From the above, it can be seen that, over the past twenty years, there has been a strong leap in the development of methods for stabilizing CEP; however, even today, it remains one of the most difficult parameters to control in any laser system.

3. Mode-Locking Regimes and Their Effect on Noise Properties

Depending on the parameters of the laser resonator, several generation regimes can be observed in USP fiber lasers. At present, there are four main regimes for stable mode-locking operation: solitons [80], stretched pulse generation [81], similaritons [82], and dissipative solitons [83]. The main resonator parameter that affects the generation regime is the total GVD value of the laser cavity. Figure 3 schematically shows a simplified dependence of the generation regime on the net-cavity GVD value. Soliton generation regime was one of the first mode-locked operations of USP fiber laser. The soliton generation was observed when the total GVD value was sufficiently negative (by negative GVD, we mean the coefficient $\beta_2 < 0$). In the region near zero of the net-cavity GVD value, the generation of stretched pulses can be obtained. Laser cavities with a value near zero of the total GVD consist of sections where the fibers have either positive or negative GVD. Due to the compensation of the cavity GVD values, a zero value of total GVD is obtained. Such lasers are referred to as dispersion-managed lasers (DM lasers). Similaritons can also be generated in the USP lasers with dispersion control but mainly with a small positive value of the net-cavity GVD. Lasers with fully positive values of the net-cavity GVD generate so-called dissipative solitons.

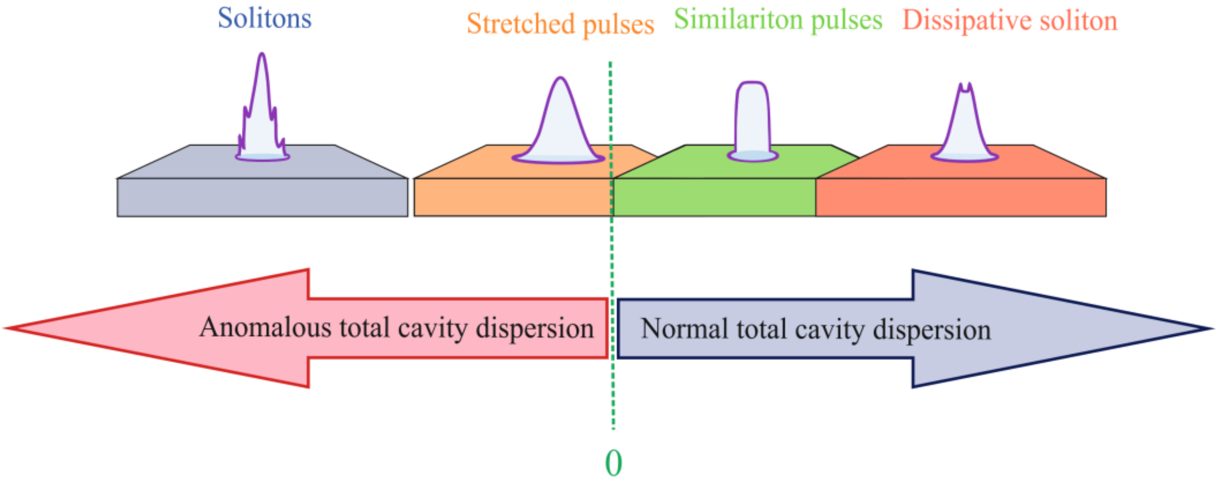

Figure 3. Simplified dependence of the generation regimes on the net-cavity total GVD value.

The GVD, which changes the pulse duration, is not the only factor affecting radiation propagation in the USP lasers cavity. Along with it, nonlinear optical effects in an optical fiber are essential factors that affect radiation stability and lead to the destruction of the pulse shape at their large values. In most cases, the dominant nonlinear effect in fiber USP lasers is self-phase modulation (SPM), which imparts a positive chirp to the pulses, just as in the case of a medium with a positive GVD value. For pulse durations <1 ps, it is necessary to take into account the first derivative of the slowly varying part of the nonlinear polarization (leading to the formation of an envelope shock wave) and the effect of stimulated Raman scattering (Raman amplification). In the case of operation near zero of the total cavity GVD of the resonator elements, it is necessary to consider the third-order dispersion β_3, which changes the pulse shape, and in some exceptional cases, the higher-order dispersion. It is convenient to use the generalized Ginzburg–Landau equation to simulate the propagation of radiation in a medium with amplification, or, as it is also called, the modified nonlinear Schrödinger equation (MNLSE), which takes into account gain and losses, as well as GVD of different orders, nonlinear effects, and the effect of saturable absorbers (SA) and spectral filters [84–87]:

$$\begin{aligned}\frac{\partial A}{\partial z} + i\frac{\beta_2(z)}{2}\frac{\partial^2 A}{\partial T^2} - \frac{\beta_3(z)}{6}\frac{\partial^3 A}{\partial T^3} = i\gamma\left(|A|^2 A + \frac{i}{\omega_0}\frac{\partial |A|^2 A}{\partial x} - T_R A\frac{\partial |A|^2}{\partial T}\right) - \Gamma A + g(z)A + \\ + g(z)\tau_g^2\frac{\partial^2 A}{\partial T^2} + \frac{1}{\Omega}\frac{\partial^2 A}{\partial T^2} + \alpha|A|^2 A + \delta|A|^4 A,\end{aligned} \tag{13}$$

where A—slowly changing amplitude of the envelope; z—coordinate of pulse propagation; T—coordinate moving with the group velocity v_g of the impulse (the so-called running coordinates), equal to $T = t - z/v_g = t - \beta_1 z$; γ—nonlinearity parameter equal to $\gamma = n_2\omega_0/cA_{eff}$, where n_2—nonlinear refractive index, ω_0—carrier circular frequency, c—speed of light in vacuum, and A_{eff}—effective mode area; T_R—is related to the slope of the Raman gain line, its value at a wavelength of 1.5 µm is 3 fs; Γ—cavity linear loss; $g(z)$—active fiber gain; τ_g^2—the lifetime of the excited state, equal to $\tau_g^2 = 2\pi c/\omega_0^2\Delta\lambda_g$, where ω_0^2—center frequency and $\Delta\lambda_g$—gain bandwidth; Ω—spectral filter width; α and

δ—terms reflecting the influence of the saturable absorber, third and fifth degrees, respectively.

Equation (13) is a generalized equation of propagation of the USPs and, in this form, is not used for modeling. More simplified versions of Equation (13) are used for calculations, which do not consider various factors. The solution to the equation can be several types of oscillations depending on the parameters of the USP lasers cavity. The pulse shape in the form of the square of the hyperbolic secant $(sech^2)$ is the solution for solitons. Additionally, solutions that satisfy the MNLSE conditions can be pulses having a chirped secant, a Gaussian shape, or a parabolic pulse shape.

Figure 4 shows a simplified diagram of the evolution of different generation modes in the USP lasers depending on the total cavity GVD and nonlinearity, but it does not consider the effect of the saturable absorber, gain, and losses. This figure illustrates the main differences in the propagation of pulses in the laser cavity for different generation modes. For example, the soliton generation retains the shape and amplitude of the pulse along the entire length of the cavity. In the stretched-pulse mode and the similariton generation, the pulse duration changes as it propagates in the cavity, the so-called "breathing" of the pulse, but for realizing the similariton generation, it is essential to have more significant nonlinearity. The behavior of dissipative solitons is close to the conduct of conservative solitons, only their generation is observed in cavities with an entirely or large positive total GVD, and the pulse duration and chirp in it change insignificantly. We discuss the features of all four generation modes in more detail in the following sections.

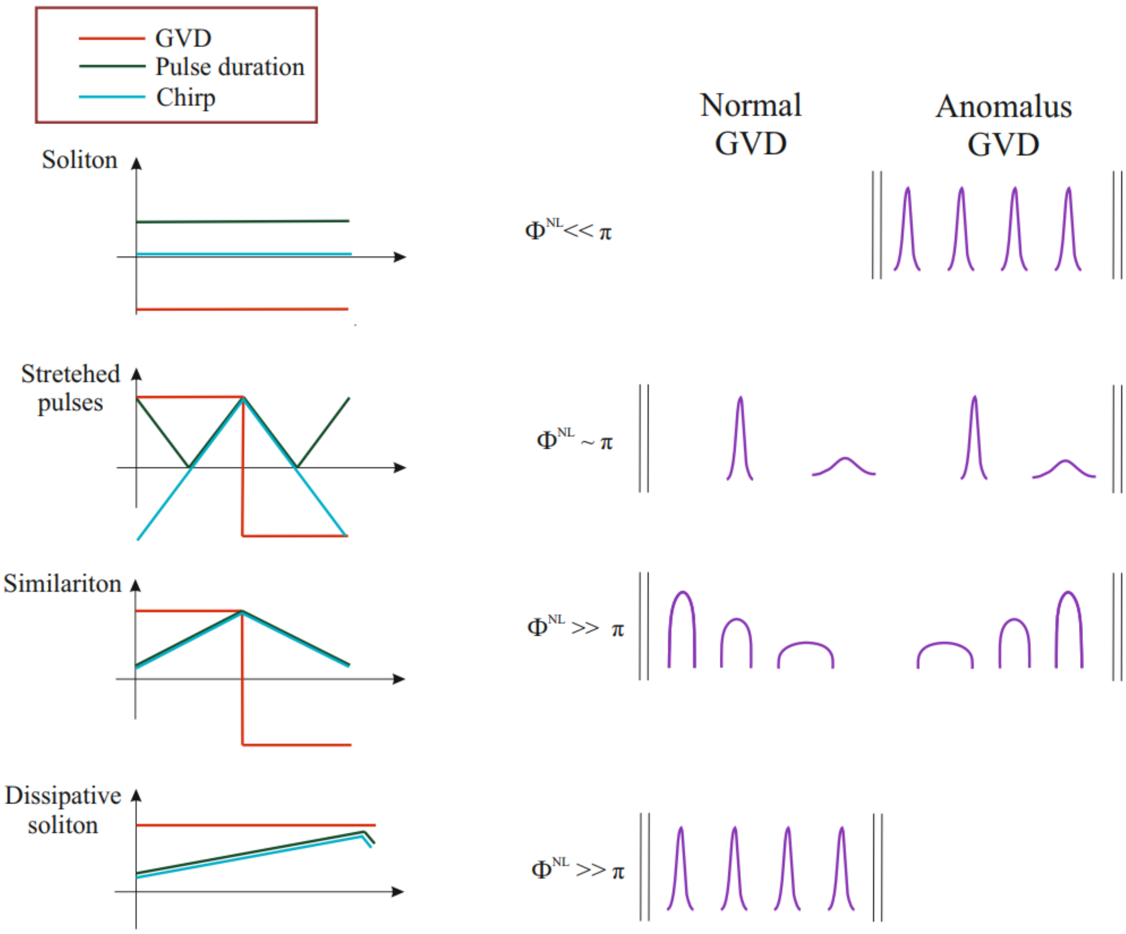

Figure 4. A simplified diagram of the evolution of pulses in resonators of different types. Double stripe shows the beginning and end of one resonator pass.

3.1. Soliton Generation Mode

The generation of solitons is observed in lasers with an entirely or significant negative (anomalous) value of the total cavity GVD. As shown in the work [88], soliton generation in an erbium USP fiber laser is observed at a value of the total cavity dispersion approximately lower than -0.04 ps^2. However, the article [89] shows that for an all-fiber thulium/holmium-doped fiber laser, the transformation of the soliton generation mode into the stretched pulses mode is carried out at zero of the total dispersion of the cavity. The balance between GVD and SPM caused by fiber nonlinearity makes it possible to obtain a generation in which the pulse retains its shape and amplitude in all propagation regions. The equal value of negative and positive phase modulation (chirp) indicates that such a pulse will not have a chirp. This behavior is similar to pulse propagation in an ideal linear dispersionless medium. For the first time, the soliton concept was introduced in 1965 [90]. The exact soliton solution of the MNLSE was demonstrated in 1971 [91]. The soliton generation mode was the first obtained in the USP lasers. The first fiber erbium laser supporting the solitons generation was demonstrated in 1980 [92], and its pulse duration was 7 ps. In a conventional soliton, Equation 13 is simplified and takes the form 8, which does not consider the GVD of higher orders, some nonlinear effects, and filtration. This is because the generation of a soliton occurs at a sufficient distance from zero of the total net cavity GVD, with pulse durations >100 fs (in most cases) [93].

$$\frac{\partial A}{\partial z} + i\frac{\beta_2(z)}{2}\frac{\partial^2 A}{\partial T^2} = i\gamma(|A|^2 A) \tag{14}$$

Equation (8) has solutions for different integer values of the parameter N:

$$N^2 = \frac{\gamma P_0 T_0^2}{|\beta_2|}, \tag{15}$$

where P_0—peak power value and T_0—pulse duration parameter equal to $T_0 \approx T_{FWHM}/1.7627$, where T_{FWHM}—the experimentally measured pulse duration at half maximum.

When N = 1, the phase modulation from GVD and SPM cancel each other out. In this case, the soliton retains its shape during propagation in a nonlinear medium. However, there is a solution of Equation 14 for >1. These cases refer to solitons of higher orders, and they change their shape with some periodicity—"breathe". The pulse shape of the fundamental soliton (N = 1) is a hyperbolic secant and has the form [52]:

$$A(t,z) = A_0 \mathrm{sech}(t/T_0)e^{i\varphi} \tag{16}$$

where $\varphi = |\beta_2|z/2T_0^2$. Neglecting the medium gain bandwidth, the energy and duration of a soliton pulse can be estimated [52]:

$$E_S = \frac{3.53\sqrt{|D_2|}}{\gamma L} \tag{17}$$

$$T_{FWHM} = \sqrt{|D_2|} \tag{18}$$

where D_2—resonator dispersion equal to $D_2 = \beta_2 L$; L—the resonator length.

There is a solution of Equation 8 for N = 1, of the form 10, and for the value β_2 > 0. Such a solution is called "dark" solitons, and it also has the form of a hyperbolic secant and was obtained experimentally [94]. "Dark" solitons are dips in continuous radiation, which have the form of hyperbolic secant.

The most important property of a soliton solution to a nonlinear equation is its stability. If, in the cases considered above, the amplitude of the soliton practically did not change, then in actual laser resonators, some elements introduce losses or gain. Under such conditions, it is no longer possible to speak of the propagation of typical solitons in USP laser resonators. The stability of a soliton manifests itself in the fact that, when a pulse propagates in a nonlinear medium with a negative GVD and with a parameter N different from an integer, the pulse tends to a soliton form, i.e., tends to the nearest integer value of the parameter N. As a result, some of its energy is scattered in the form of dispersive waves, which are stored in the cavity in the case of a laser. In the USP lasers, part of the radiation leaves it through the splitter after each passage by the pulse. The peak power sharply decreases, and, consequently, the balance between the nonlinearity of the medium and the GVD is violated. The soliton seeks to return its parameters to the nearest integer value of the parameter N and transfer part of its energy to dispersive waves, which, as in the case of the main pulse, circulate in the resonator. As a result, in the envelope of the optical spectrum of the USP laser operating in the soliton generation mode, side peaks, or as they are also called Kelly sidebands [95], will be observed, which have the form shown in Figure 5 [96].

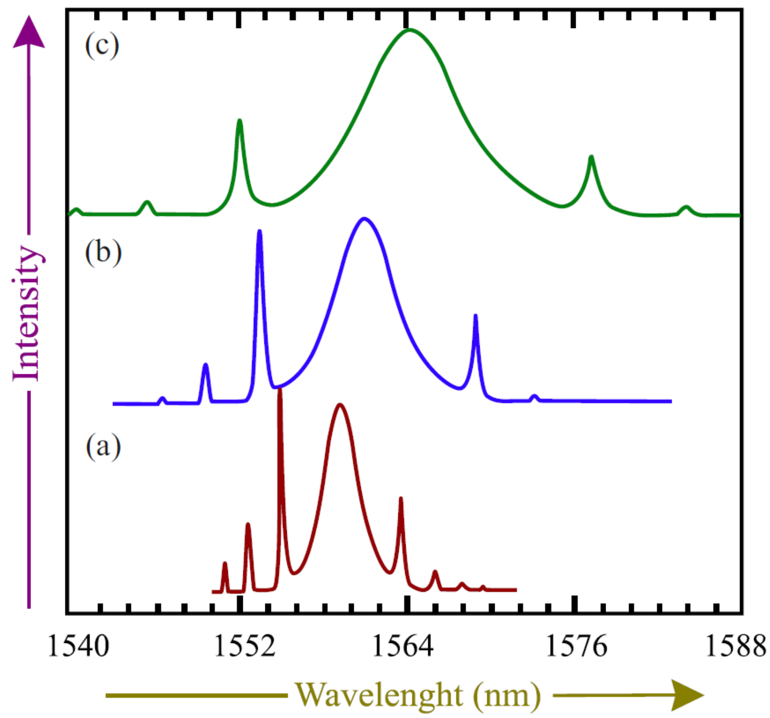

Figure 5. Optical spectral envelopes obtained in lasers with different cavity lengths. Pulse duration and total dispersion for: (a) 1130 fs, 616 fs/nm; (b) 470 fs, 216 fs/nm; (c) 300 fs, 79 fs/nm.

Dispersion waves propagate following the linear dispersion coefficient β_D, while the soliton following the nonlinear dispersion coefficient, which considers the influence of the SPM on the β_S pulse [97]. Each time a soliton passes through the cavity, it generates dispersive waves that interfere with each other. The growth of the dispersion wave amplitude depends on the phase, each new phase formed during the passage of the dispersive wave. As a result, the strongest dispersive waves are generated when its phase becomes a multiple of the 2π phase of the soliton (i.e., each new dispersive wave is in phase with the one already propagating in the resonator). Mathematically, it looks like this [98]:

$$\beta_S(\widetilde{\omega}_m)L = \beta_D(\widetilde{\omega}_m)L + 2m\pi \tag{19}$$

where L—resonator length; m—integer; $\widetilde{\omega}_m$—offset of the m-th side peak from the center frequency; β_S and β_D—average dispersion values for the soliton and dispersive wave, respectively; $\beta_D L$—total net cavity dispersion. Expanding β_D and β_S in a Taylor series [97] and substituting them into Equation (19), we obtain an equation that can be used to predict the positions of the side peaks:

$$m = \frac{\beta_2 L}{4\pi}\left(T_0^{-2} - \widetilde{\omega}_m^2\right) - \frac{\beta_3 L}{12\pi}\widetilde{\omega}_m^3 \tag{20}$$

Energy transfer to side peaks is the main limitation of the minimum pulse duration attainable in soliton lasers. The energy and pulse duration in lasers generating soliton-like pulses is inversely proportional [99]; as a result, the optimal pulse duration for such lasers are a few picoseconds, where the pulse energy can be around 10 nJ [100].

In Equation (6), to find the jitter, in the soliton generation mode, the values of the parameters I_ω and I_t are equal $I_\omega = 0.2647\mathrm{E}\Delta\Omega_p^2$ and $I_t = 0.2647\mathrm{E}\Delta t^2$, where Δt is the pulse full width at half maximum. Taking $C = 1$, since the soliton has no chirp, and substituting the values of I_ω and I_t into Equation (6), then for $T \gg \tau_g$ the equation has the form:

$$J^2 = 0.53\frac{2h\nu}{E^2}(g-1)\left[\frac{4D_2^2\Omega_g^4}{g^2\Delta\Omega_p^2} + \Delta t^2\right]\frac{T}{T_R} \tag{21}$$

As can be seen from Equation (21), jitter is greatly influenced by the laser total net cavity GVD, pulse parameters, and medium characteristics. The soliton generation mode is formed at large negative values of the total net cavity GVD and, on average, does not have the best values of the pulse duration and the width of the optical spectrum envelope, which negatively affects the jitter value. Additionally, the pulse energy of a soliton laser is limited. The main advantage of the soliton mode is the stability of the pulse generation. The use of this generation mode to implement fiber USP laser with high requirements for the stability of the amplitude and time characteristics of the output radiation will not be optimal. Therefore, we considered other generation modes.

It is necessary to note such a generation mode as the multibound solitons (MBSs) [101–103]. MBS generation regime [104], soliton molecules [105], and soliton crystals [106] involve a bound state of multiple optical pulses that propagate with a fixed temporal separation through optical fibers. The appearance of a multibound state can be caused by several reasons, but it is always based on the effective interaction of solitons in highly nonlinear systems, such as fiber lasers with passive mode-locking. At the same time, the energy of such systems is quantization subject, due to the soliton area theorem, which ultimately leads to the formation of several pulses in the resonator [107]. There are three main bound state formation mechanisms that lead to the quantization of energy in the resonator. The first mechanism is associated with pulse splitting due to a limited gain band [108]. In highly nonlinear cavities, due to the effect of SPM and XPM, the spectrum of a USP can be broadened so much that some frequency components xtend beyond the bandwidth of the gain medium. Because of this, the pulse can be split into several bound pulses, with wider spectra, to avoid increasing losses. The second mechanism for the generation of bound solitons can be described as follows: when a soliton whose order does not exactly correspond to the fundamental one passes through a fiber with anomalous chromatic dispersion, it can decay into several higher-order solitons (N > 1). However, the presence of uncompensated higher-order dispersion leads to radiation of dispersive waves [109]. In this case, in an amplifying medium with strong pumping, some of the dispersive waves can acquire sufficient amplification to grow and evolve into a new pulse with a width and amplitude determined by the parameters of the fiber resonator. The third mechanism for the occurrence of a bound state is related to the transmittance of a cavity formed by a nonlinear polarization rotation (NPR) or a nonlinear fiber loop mirror (NFLM). Due to the sinusoidal characteristic of the resonator transmittance in both of these methods, there are two different modes of operation in one period of the transmission curve [110]. In the first part, the transmittance increases with increasing intensity, and in the second part, it decreases with increasing intensity. The peak of the transmission curve is also the transition point between two modes: saturable absorption and saturable gain. In the NPR method, by fine-tuning the linear phase delay, by means of polarization controllers, it is possible to shift the switching point between the two modes. In this case, as a result of the resonator feedback, the peak power of the soliton, which is for the quantization of the pulse energy, will be limited.

3.2. Stretched Pulses Generation Mode

The stretched pulse generation is realized with the help of GVD control in the cavity and has advantages over the usual soliton generation mode in the pulse duration and energy. The first experimental data on an all-fiber ring laser generating stretched pulses were obtained in 1993 [111]. Dispersion control consists of using fibers with both negative and positive GVD in the laser cavity. The main feature of this generation mode is the ability to reduce nonlinear effects by changing the pulse duration inside the cavity. A pulse propagating in such a resonator "breathes" and has a large average pulse duration compared to the soliton generation mode. Reducing the average pulse duration reduces the peak radiation power and, accordingly, the nonlinear effects in the cavity that limit the pulse energy. An important feature of stretched pulses is the change in the chirp along the cavity length. The maximum nonlinear phase incursion does not exceed π. When solving Equation (13) with the assumptions that are valid for the stretched pulses generation, it can be found that the pulses in this mode have a Gaussian pulse shape:

$$A(t) = A_0 exp\left(-\frac{t^2}{2T_0^2}\right) \tag{22}$$

where for Gaussian pulses $T_0 = T_{FWHM}/\sqrt{4\ln(2)} \approx T_{FWHM}/1.665$.

By analogy with Equations (17) and (18), one can express the estimated expressions for the energy and pulse duration for the stretched (Gaussian) pulse mode [52]:

$$E_S = \frac{4.47\sqrt{|D_2|}}{\gamma L} \tag{23}$$

$$T_{FWHM} = 0.66\sqrt{|D_2|} \tag{24}$$

where D_2 is the total net cavity GVD with a positive GVD value, defined as $D_2 = \beta_2 z$, where z is the length of the fiber with positive dispersion.

A typical stretched pulse laser layout is shown in Figure 6 [112]. It includes two fiber sections, one that is an active fiber with a positive GVD value and the other is a fiber with a negative GVD value. Propagating through the resonator, the pulse duration changes and reaches a minimum value at two points of the resonator. The total value of the GVD of the cavity elements strongly affects the input characteristics of the laser. Theoretically, the highest energy and shortest duration can be achieved with a positive value of the total net cavity GVD. In such a scheme, the pulse duration can vary by several orders of magnitude, and the more significant this ratio, the less undesirable nonlinear effects. However, the best results are observed at a weakly positive value of the total GVD, since at large values of the positive total GVD of the resonator elements, pulse instability and a strongly asymmetric spectrum are observed [88]. With a strongly negative dispersion, a soliton generation mode is observed with a $sech^2$ pulse shape and Kelly peaks. The optimal position of the output splitter is the position immediately after the active fiber with positive dispersion [81]. This is most likely because, in such a configuration, the influence of soliton effects on the pulse decreases, since only part of the energy enters into a fiber with negative dispersion. The typical pulse energy for the stretched pulse mode is 1 nJ, but there are publications where the pulse energy reached 3 nJ [113]. The pulse duration is approximately from 70 to 100 fs, although there are works in which the pulse duration gets 47 fs [114].

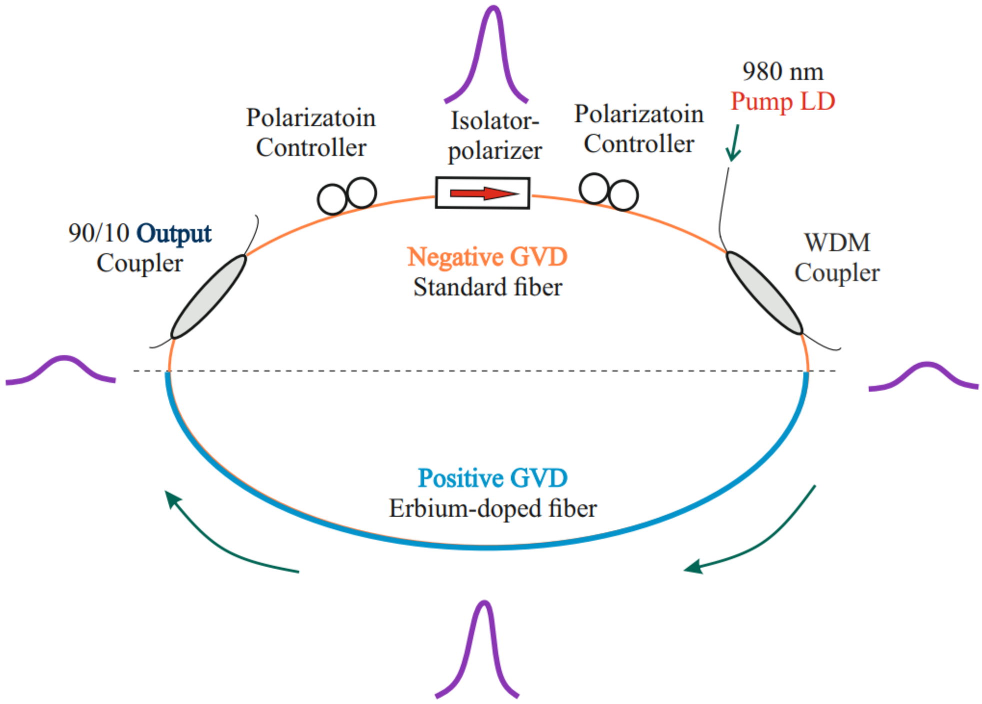

Figure 6. Diagram of an all-fiber laser operating in stretched pulses generation.

When operating in the stretched pulse generation mode, in Equation (6), to find the jitter, the values of the parameters I_ω and I_t will be equal $I_\omega = 0.2647\text{E}\Delta\Omega_p^2$ and $I_t = 0.2647\text{E}\Delta t_{max}^2$, where Δt_{max} is the maximum width of the pulse duration by half-height. Taking the chirp as the maximum value, and substituting the values of I_ω and I_t in Equation (6), then for $T \gg \tau_g$ the equation has the form:

$$J^2 = 0.36\frac{2h\nu}{E^2}(g-1)\left[C\frac{4D_2^2\Omega_g^4}{g^2\Delta\Omega_p^2} + \Delta t_{max}^2\right]\frac{T}{T_R} \tag{25}$$

Equation (25) shows that both in solitons and stretched pulses generation modes, the jitter is greatly influenced by the total GVD value, the pulse parameters, and the medium's characteristics. The total GVD of the elements of a resonator operating in the stretched pulses generation mode can be close to zero, and the envelope of the optical spectrum of radiation is usually wider than that of solitons, which leads to a much lower value of jitter. However, the stretched pulse generation mode is subject to destruction at high pulse energies, as in the soliton generation mode.

3.3. Similariton Pulses Generation Mode

The similariton generation mode is achieved with a positive value of the total GVD of the laser cavity elements with dispersion control. This generation mode has a parabolic pulse shape and a parabolic spectrum. For the first time, a theoretical analysis of the propagation of parabolic pulses in fibers with a positive GVD value and strong gain was demonstrated in 1993 [115], where it was argued that these pulses are not subject to destruction at high pulse energies. In 2000, parabolic pulses with a linear chirp were implemented in a high-gain ytterbium fiber amplifier [116]. Four years later, a USP laser operating in the similariton generation mode was implemented [82,117].

Similaritons or parabolic impulses are an asymptotic solution of the nonlinear Schrödinger Equation (13), and approximately have the form [52]:

$$A(t) = A_0\left[1-\left(\frac{t}{T_0}\right)^2\right]^{1/2} exp\left(-iC\frac{t^2}{2T_0^2}\right), \tag{26}$$

where $T_0 = T_{FWHM}/\sqrt{2} \approx T_{FWHM}/1.414$; C—chirp parameter $C = \pi T_{FWHM}\Delta\nu \gg 1$, where $\Delta\nu$—the width of the emission spectrum in frequencies. If the phase incursion inside the resonator is π, then the expression for the pulse energy has the form:

$$E_S = \frac{4.47 D_2 \Delta\Omega}{\gamma L} C. \tag{27}$$

Similaritons develop in a fiber with a positive GVD value, high gain, and nonlinearity during propagation along which the optical spectrum broadens. In most cases, for similaritons observed in resonators, the total GVD is greater than the total GVD of resonators generating stretched pulses; however, in some cases, both similaritons and stretched pulses can be generated in one resonator (with different adjustments). A cavity section with a negative GVD value is required to implement a laser, and so that the similariton does not transform into a soliton, this section should not have nonlinearity; therefore, prisms or diffraction gratings are used for this. The similariton generation remains stable as long as the width of the envelope of the optical spectrum of the pulse does not exceed the width of the optical gain spectrum of the active medium [118]. Since a similariton tends to broaden the spectrum when propagating in an active medium, to obtain stable laser generation, which implies feedback, it is necessary to organize a mechanism that limits the broadening of the pulse spectrum. Most often, such a limiter is a spectral filter.

The main disadvantage of the solitons and stretched pulses is energy limitation due to a high level of nonlinearity. Self-phase modulation can cause high-energy pulses to change shape, become asymmetric, or even decay into multiple pulses. Similaritons, on the other hand, are capable of reaching high energy levels without breaking the pulse [116]. They can exist at a much higher SPM (>π) than stretched or soliton pulses. To date, the peak power of a laser operating in the similariton generation mode can exceed the peak power of a laser operating in the stretched pulse mode by a factor of 6 [85]. Similaritons have a parabolic shape throughout the cavity and at the output. An ideal similariton has a linear chirp, making it easy to organize the compression of the pulse after it leaves the cavity. A similariton has one place of minimum duration in the cavity, in contrast to the stretched pulse mode, where there are two. The minimum pulse duration is located immediately after the element with negative dispersion in the laser cavity and is not spectrally limited in this place.

An important difference between the stretched pulses and similaritons is that the similariton compression requires a larger negative dispersion than the negative GVD inside the laser cavity. Since the stretched pulse mode has two minima in the cavity, to achieve spectral limitation, it needs a lower total compressor GVD. This factor can be used to determine the generation mode, since parabolic shapes are insufficient in determining the similaritons generation [119]. At present, erbium fiber lasers are operating in the similariton mode with a pulse energy of 6.2 nJ and a duration of 64 fs [120].

When operating in the similariton mode, in Equation (6), to find a jitter, the parameter values I_ω and I_t are equal $I_\omega = 0.2\mathrm{E}\Delta\Omega_p^2$ and $I_t = 0.2\mathrm{E}\Delta t^2$, and Δt_{max} is the maximum width of the pulse duration by FWHM. Taking C as the maximum chirp value, and substituting the values and I_t into Equation (6), then for $T \gg \tau_g$ the equation has the form:

$$J^2 = 0.4\frac{2h\nu}{E^2}(g-1)\left[C\frac{4D_2^2\Omega_g^4}{g^2\Delta\Omega_p^2} + \Delta t_{max}^2\right]\frac{T}{T_R}. \tag{28}$$

As can be seen from Equation (28), as for other generation modes, for the similariton generation, the jitter is greatly influenced by the total net cavity GVD of, the pulse parameters, and the medium's characteristics. The total net cavity group velocity dispersion of a fiber laser operating in the similariton mode can be close to zero. The width of the optical spectrum envelope is comparable to the optical spectrum envelope width of a laser operating in the stretched pulse generation. This generation mode has the most significant number of advantages for implementing fiber USP laser with high requirements for the stability of the amplitude and temporal characteristics of the output radiation. However, it is necessary to consider the fourth mode of generation of fiber USP lasers.

3.4. Dissipative Soliton Generation Mode

The generation of dissipative solitons is mainly observed in resonators, which are of great importance for the purely positive total GVD of the resonator. However, dissipative solitons can also be encountered in lasers with dispersion control but with a vast overall positive value of the total net cavity GVD. Unlike a conventional soliton, this pulse undergoes amplification and losses in the cavity. The stable generation of a laser in the mode of dissipative solitons requires a spectral filter in the cavity to limit the growth of the laser spectrum [121]. The features of pulses in this generation mode are a significant value of the chirp and its positive sign (since the dispersion of the cavity is positive). The first erbium fiber laser generating dissipative solitons was implemented in 2006 [122].

Dissipative solitons, as in the case of the previous generation modes, are a solution to Equation (13), and the approximate solution has the form [85]:

$$A(t,z) = A_0 \mathrm{sech}(t/T_0) e^{i\beta_2 \ln(sech(\frac{t}{T_0}))+i\theta z} \tag{29}$$

As seen from Equation (23), the pulse shape is very similar to the soliton (Equation (10)). The difference lies in the presence of a chirp. Another feature of dissipative solitons is pulse "breathing," similar to the generation of stretched pulses, but this "breathing" is associated with filtering the laser spectrum and not with a GVD value changing. The maximum pulse duration ratio in the cavity to the minimum one is from 5 to 6, which is much less than in the case of stretched pulse generation. To date, in erbium fiber lasers operating in the dissipative soliton generation mode, a pulse duration after compression of 80 fs was achieved with a peak pulse power of 200 kW and an average power of 1 W, while the total cavity dispersion was ~0.05 ps^2 [123].

For the generation of dissipative solitons, Equation (28) is applicable to determine the jitter. In this case, the total net cavity GVD is far from zero, as in the case of ordinary solitons, only towards the positive value of the GVD.

3.5. Selection of the Optimal Mode-Locking Regime

Based on the analysis of the generation modes of fiber USP lasers, a summary in Table 2 was compiled, which reflects the main output characteristics of the radiation and the parameters of laser resonators at various generation modes. Typical values are indicated for each mode. As mentioned above, the main parameter characterizing the stability of time characteristics is the jitter, which depends on the USP laser total GVD.

Table 2. Comparison of the main characteristics of various generation modes in fiber USP lasers.

Parameter	Soliton	Stretched Pulses	Similariton	Dissipative Soliton
Total GVD of the resonator elements	<0	close to 0	close to 0	>0
Maximum pulse energy	limited	limited	not limited	not limited
Minimum pulse duration	~1 ps	tens of femtoseconds	tens of femtoseconds	tens of femtoseconds

Figure 7 shows the calculation of the dependence of the jitter of the total net cavity GVD for each generation mode of the fiber USP laser. As shown in Figure 6, the smallest jitter value is observed at zero of the total cavity GVD for the stretched pulse generation and the similariton generation. However, for the similariton mode, the jitter dependence on the total net cavity GVD has a lower proportionality coefficient than the stretched pulse generation mode.

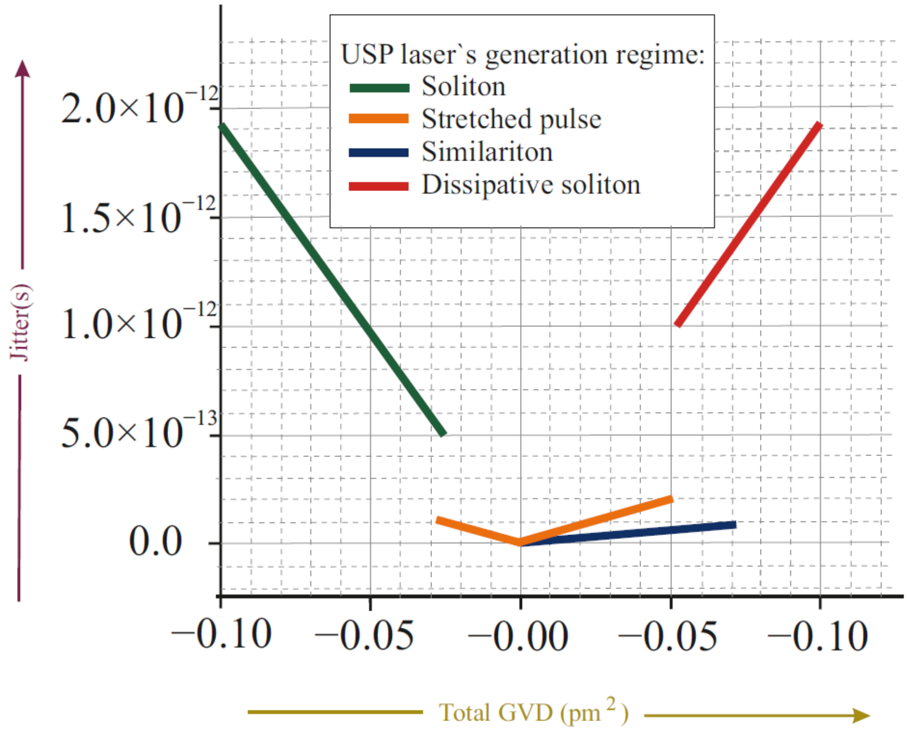

Figure 7. Calculation of the dependence of the jitter value on the total GVD of the USP laser resonator elements.

A laser operating in the similariton mode, as in the case of a laser operating in a stretched-pulse mode, is well suited for implementing a highly stable fiber USP laser with a total GVD of the cavity elements close to zero. However, in contrast to the stretched-pulse generation mode, the similaritons generation mode does not have a theoretical limitation on the pulse energy, which makes it possible to achieve more excellent stability of the amplitude characteristics of the USP lasers output radiation. Additionally, based on the analysis carried out above, it can be concluded that at the same values of the total GVD of a fiber USP laser, different modes can be generated in it. This is especially pronounced in the region of a small positive total net-cavity second-order dispersion. Since the similaritons generation mode is formed in the region of a small positive total dispersion of the cavity, a technique is needed to identify the generation mode by the output characteristics of the laser radiation.

4. Classification and Comparative Analysis of Structural and Functional Fiber USP Laser Schemes

A critical component of a USP laser cavity is the mode-locking mechanism used to generate and shape the pulses. The used mode-locking mechanism will determine the minimum pulse duration and the minimum lasing trigger threshold, pulse repetition rate, and maximum pulse energy. The influence of the mode-locking mechanism on the stability of the amplitude and time characteristics of lasing cannot be ignored. USPs in all modern fiber lasers are generated using a passive mode-locking mechanism. Passive mode-locking was realized several years later than active mode-locking [124,125]. The fundamental difference between this mode-locking technique is the lack of control over the modulator using external signals. For the development of passive mode-locking, it is necessary that lasing begins immediately with a large number of modes in the cavity. An important part of the USP lasers cavity with passive mode-locking is an element with a nonlinear transmission—a saturable absorber. It is when radiation passes through this element that the temporal intensity profile changes. Low-intensive pulses are further attenuated in a saturable absorber, while high-intensive pulses are transmitted with lower losses. As a result of the combined action of the active medium and the saturable absorber, fluctuation pulses are discriminated (mode discrimination). In the end, one pulse remains in the cavity. Figure 8 shows the development of passive mode locking over time [126].

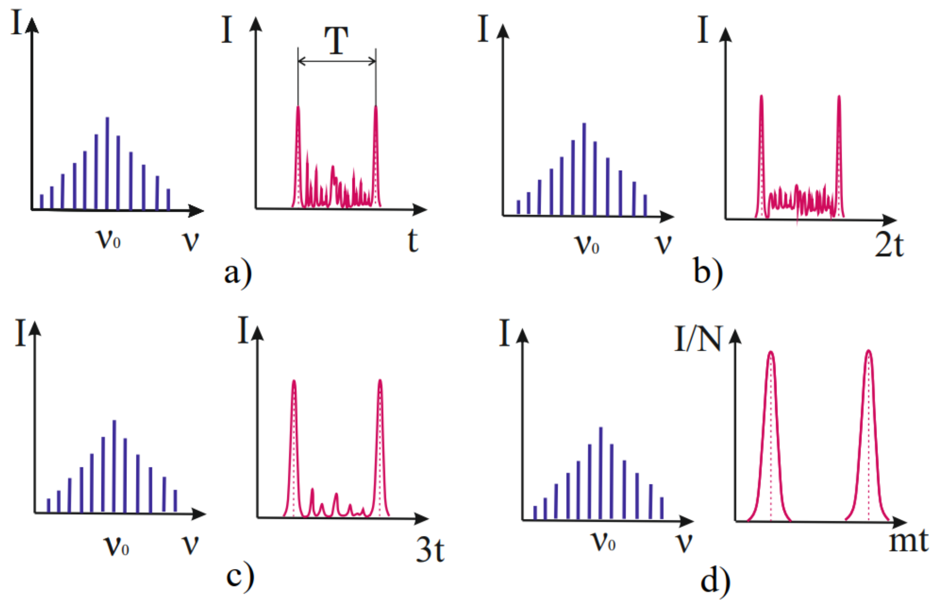

Figure 8. The pulse formation occurs at once at all frequencies of the laser band: (**a**) shows the evolution of the laser radiation parameters after the first pass of the cavity; (**b**,**c**) after the second and third, respectively; (**d**) already shows the result of the saturable absorber after a large amount of radiation passes through the cavity.

Pulse shape changes when it passes through the transparency window of the SA after a single pulse remains on the period. The saturable absorber "cuts" the leading and trailing edges of the pulse until the pulse duration is close to the relaxation time of the SA. The process of decreasing the duration of the leading and trailing edges (left pulse) and smoothing out fluctuation pulses of low intensity (right pulse) is shown in Figure 9.

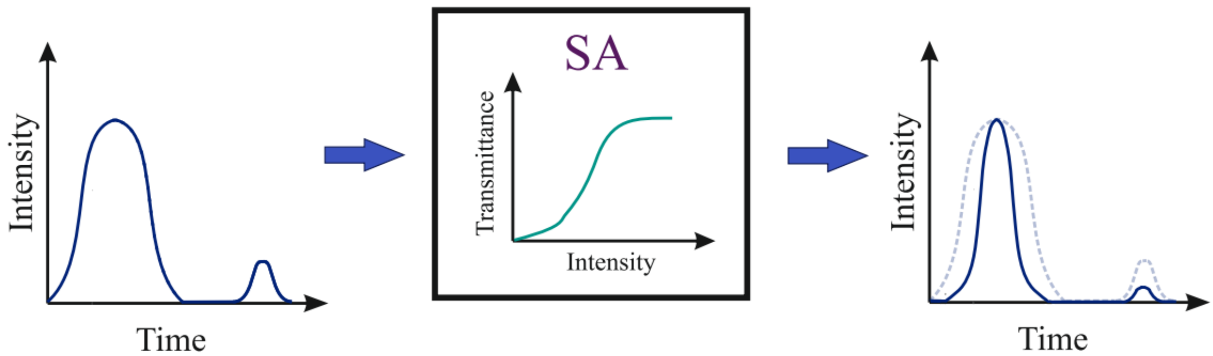

Figure 9. The processes of cutting the leading and trailing edges (left pulse) and smoothing fluctuation pulses of low intensity (right pulse).

The main characteristics of saturable absorbers are:

- Modulation depth is the maximum change in nonlinear absorption (or reflection) caused by radiation incident on the absorber;
- Saturation energy is the energy required to clear the absorber by a factor of $1/e$ ($\approx$37%);
- The recovery (relaxation) time is the time during which the absorption is restored e times (2.718 times) after the passage of the pulse;

- Non-saturable losses are unwanted losses that do not participate in the nonlinear absorption process;
- Service life is the time during which the saturable absorber provides the required modulation depth and other properties;
- Moreover, note such characteristics as the optical damage threshold and GVD.

The following types of saturable absorbers are most commonly used in fiber lasers:

- An absorber using nonlinear polarization evolution (NEP) in a fiber [127,128];
- Nonlinear active loop mirror [129–131] or nonlinear optical loop mirror [132,133];
- Graded index multimode fiber (GIMF) as saturable absorber induced by nonlinear multimodal interference (NL-MML) [134,135];
- Semiconductor saturable-absorber mirror [136,137];
- Carbon nanostructures [138,139];
- Two-dimensional materials, such as bismuthine [140], black phosphorus (BP) [141], topological insulator (TI) [142,143], and others [144–146].

Natural SAs can be distinguished among the designated types of saturable absorbers. A natural SA is semiconductor saturable-absorber mirror, carbon nanostructures, and other 2D materials. An absorber using an NEP in a fiber, an annular fiber mirror with an active or passive fiber in the ring, and GIMF is called artificial SA. Artificial methods can also reduce losses for more intense radiation, but they do not contain absorbing substances as such. As shown above, the generation mode of the USP fiber laser mainly depends on the total cavity dispersion. Various materials used as SA have almost no significant effect on the generation mode. A small effect of an SA on the generation mode is possible, provided that it has a narrow spectral bandwidth of operation and behaves as a spectral filter. Let us classify the schemes of fiber laser cavities according to SAs, since they play one of the critical roles in organizing the generation of USPs.

4.1. Natural Saturable Absorbers

Dyes were the first saturable absorbers used in lasers [125]. The principle of operation of a typical SA is that radiation entering the substance is absorbed if the photon energy is sufficient to transfer the charge carrier from the valence band to the conduction band (for semiconductors) or from the ground state to the excited state (for laser media). At the low intensity of optical radiation, the population of the conduction band or the number of excited atoms is small, and the absorption remains unsaturated. At the high intensity of optical radiation, charge carriers are accumulated in the conduction band or, for laser media, all atoms are in an excited state. As a result, another transition to an excited state becomes more complex, and saturation sets in, which leads to enlightenment. The use of a natural saturable absorber, for example, a dye, has one fundamental drawback. It is necessary to have a sufficiently short relaxation time, and the shorter the relaxation time, the shorter the pulse duration can be obtained. However, a short relaxation time means that the high intensity of the fluctuation ejection is required for the SA to operate. Since lasing with passive mode-locking starts by amplifying spontaneous fluctuations, whose intensity is insufficient for the appearance of saturable absorption, this does not allow starting mode-locking.

This contradiction was overcome only with the advent of new types of SAs. The first absorbers were semiconductor saturable-absorber mirrors. The main difference between these materials is the presence of two relaxation time components — fast and slow. After saturation, absorption is restored in several stages with different relaxation times. The first process is associated with the intraband thermal relaxation of electrons and the molecular lattice of the material. The relaxation time, in this case at room temperature, is tens of femtoseconds. The second relaxation process is associated with the transition of electrons from the conduction band to the valence band. The duration of this process is several nanoseconds. When electrons enter the energy levels caused by defects or impurities, the relaxation time (liberation of the conduction band from electrons) in this case can range from hundreds of femtoseconds to hundreds of picoseconds [147]. Therefore, the lifetime of charge carriers depends on the purity of the material and the growth conditions. Defects are specially created using low-temperature growth [148] or ion bombardment [149] to reduce the relaxation time. Single-walled carbon nanotubes (SWCNTs) have optical properties similar to semiconductor absorbing mirrors, but they lack intraband relaxation [150].

When saturable absorbers are used, several modes of laser generation can be observed. The Q-switching mode, which is mainly obtained when using a saturable absorber with a long relaxation time, is shown in Figure 10b. Figure 10c shows the transient generation mode—Q-switched mode with mode-locking. Figure 10d shows the continuous mode-locking.

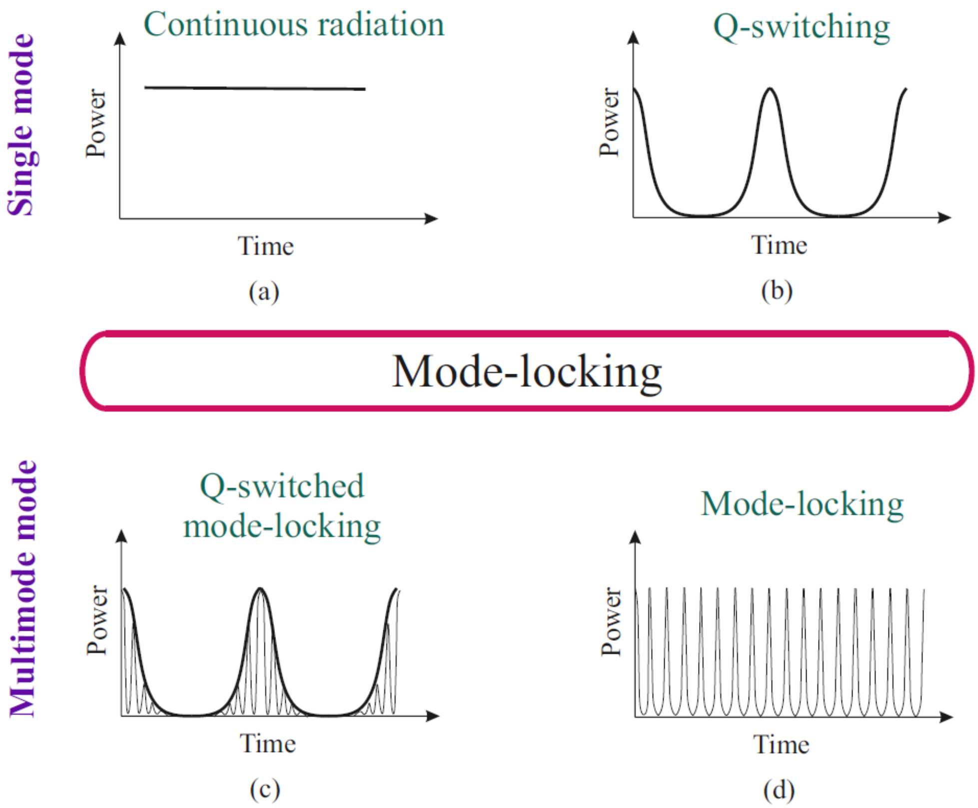

Figure 10. Various modes of operation of lasers using saturable absorbers: (**a**) continuous lasing; (**b**) Q-switching mode; (**c**) Q-switched mode with mode-locking; (**d**) mode-locking.

4.2. Semiconductor Anti-Reflective Absorber with a Bragg Mirror (SESAM)

Let us consider the principle of operation of a semiconductor SA with a Bragg mirror. The first fiber laser using a semiconductor saturable absorber mirror (SESAM, semiconductor saturable absorber mirror, or SBR, saturable Bragg reflector; SBR is a type of SESAM, and at the moment, most SESAM are of the SBR type) appeared in 1992 [136], although the first passive mode-locking using a saturable absorber was demonstrated in 1966 in a solid-state laser [125]. The use of SESAM makes it possible to obtain lasing in a passively mode-locked laser with pulse duration from several picoseconds to tens of femtoseconds and also makes it possible to obtain nanosecond pulses in the Q-switched mode.

A semiconductor saturable absorber is usually integrated with a semiconductor, dielectric or metal mirror, forming a semiconductor saturable mirror. Figure 11 schematically shows a typical SESAM structure. Quarter-wave AlA/GaA layers form a distributed Bragg reflector. The semiconductor material provides absorption. The energy gap is set following the wavelength of the optical radiation. It is usually embedded in a semiconductor material with a higher bandgap that does not absorb the optical signal. The entire absorber region can consist of several layers of quantum wells (QW), representing the so-called multiple quantum well (MQW) structure. For wavelengths of less than 1.1 μm, the absorption region consists of GaInA(P)/GaA layers deposited on a GaA/AlA Bragg reflector. For wavelengths longer than 1.3 µm, quantum wells can be made from GaInAsP. Another approach is to incorporate nitrogen into GaInAs to reduce the quaternary bandgap and prepare GaInNA/GaA quantum wells on GaA/AlA lattices. Such a heterostructure has a wide operating wavelength range, from 0.94 to 1.55 µm (or even wider), representing a significant spectral expansion of GaA technology. The absorbing layers are usually placed at field maximum (antinodes of a standing wave) for enhanced interaction. The production of SESAM technology is well established and can be carried out either with molecular beam epitaxy (MBE) or with metal–organic chemical vapor deposition (MOVPD). The absorbing section can be enclosed in a Fabry–Perot cavity forming the resonant absorber [151]. The semiconductor mirror can be chirped and used to compensate for the group-velocity dispersion in the cavity.

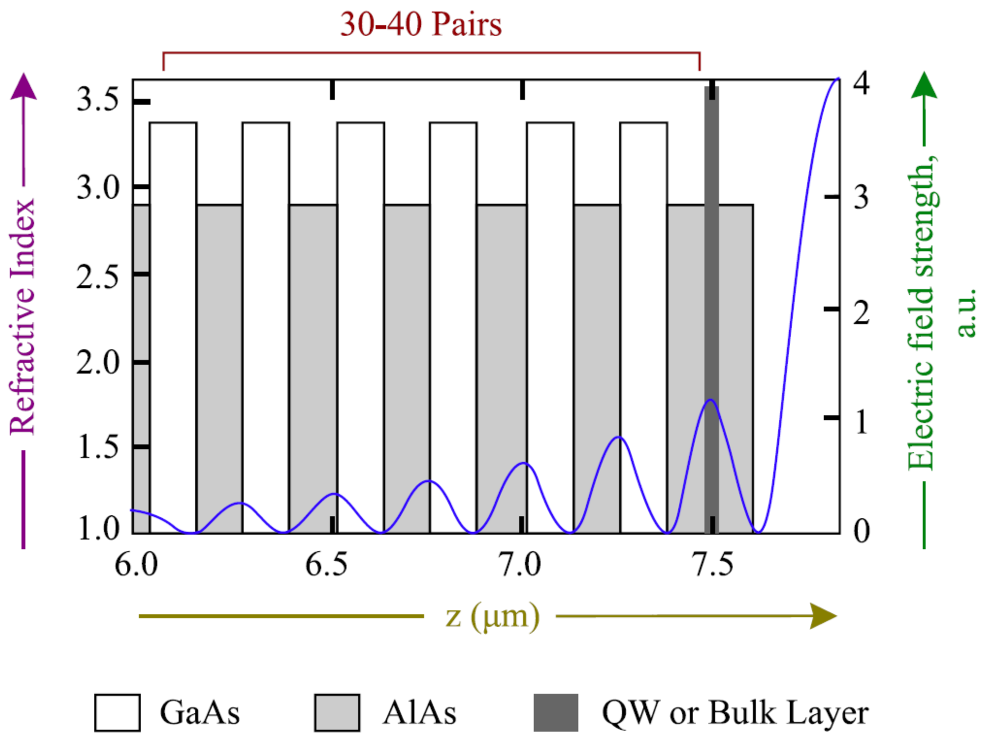

Figure 11. Scheme of a typical semiconductor saturable absorber.

After saturation, the absorption in the semiconductor saturable absorber is restored in several stages with different relaxation times. The first process is associated with the intraband thermal relaxation of electrons and the molecular lattice of the material. The relaxation time, in this case at room temperature, is tens of femtoseconds. The second relaxation process is associated with the transition of electrons from the conduction band to the valence band. The duration of this process is several nanoseconds. The relaxation time (relaxation of the conduction band from electrons) decreases when electrons enter the energy levels caused by defects or impurities [147]. Therefore, the lifetime of charge carriers depends on the purity of the material and the growth conditions. Defects are specially created using low-temperature growth [148] or ion bombardment [149] to reduce the relaxation time. The typical relaxation dynamics of a semiconductor saturable absorber are shown in Figure 12.

The use of a semiconductor SA is possible both in solid-state lasers and fiber lasers. A typical linear scheme of fiber USP lasers using SESAM is shown in Figure 13.

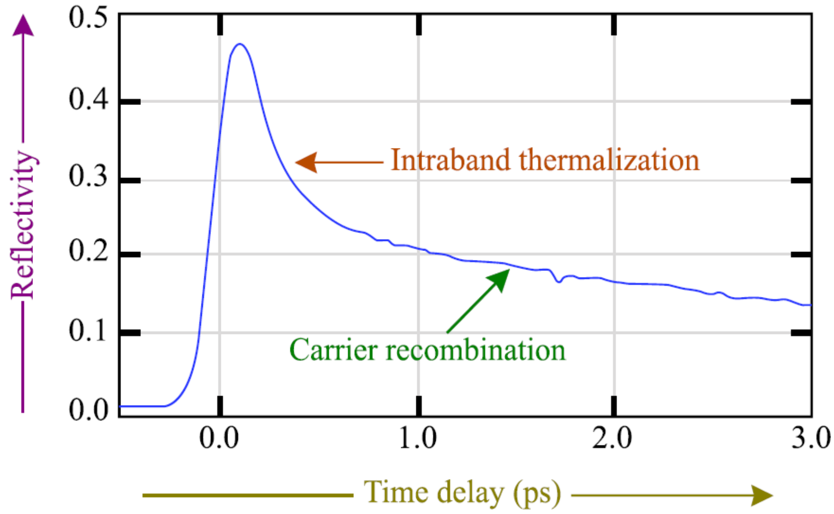

Figure 12. Typical relaxation dynamics of a semiconductor saturable absorber.

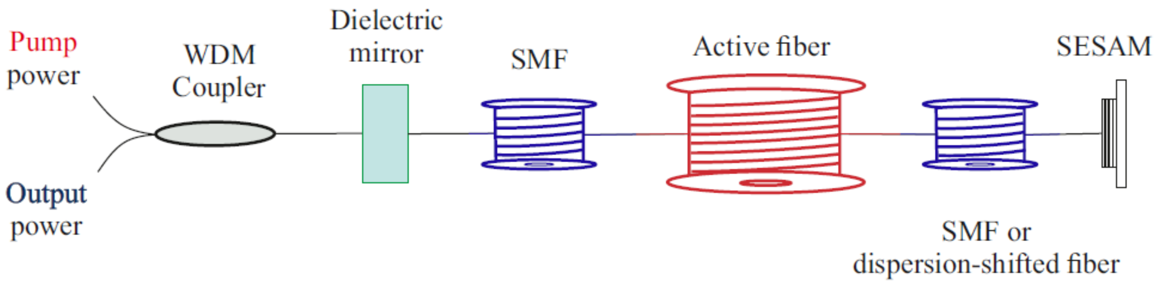

Figure 13. Typical linear mode-locked fiber cavity using SESAM.

An advantage of this scheme can be considered the possibility of creating lasers with a short cavity length to obtain a high-pulse repetition rate; there are works where lasers with a frequency from 500 to 3000 MHz were demonstrated [152,153] with different efficiency. In a linear scheme using SESAM, a soliton generation mode with a minimum pulse duration of 180 fs exhibits a timing jitter as low as 20 fs over a frequency range of 1 kHz–10 MHz [152] and a generation mode of stretched pulses with a duration of 135 fs was demonstrated [154]. Figure 14 shows a ring scheme of a USP fiber laser cavity using SESAM.

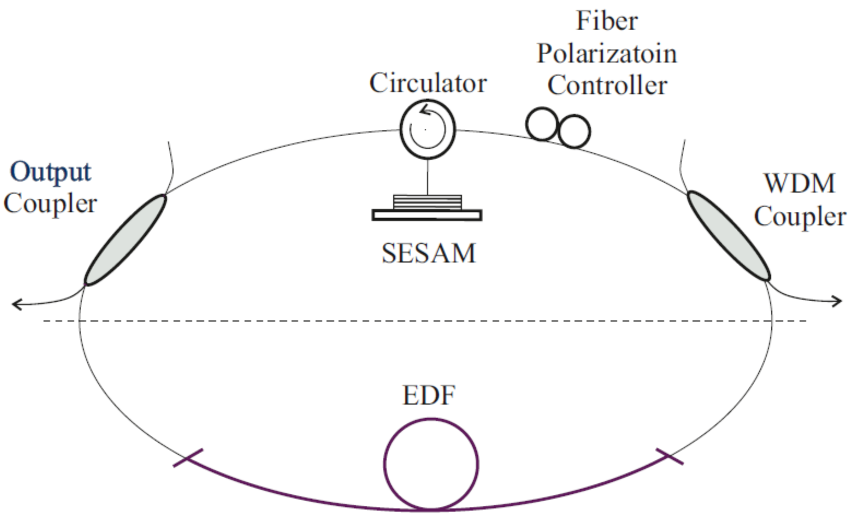

Figure 14. Ring scheme of the fiber USP lasers resonator using SESAM.

4.3. Carbon Nanostructure as a Saturable Absorber

The first SWCNTs were synthesized in the early 1990s. Their structure and properties have shown that SWCNTs can become well-saturable absorbers in the mid-IR range [155,156]. The first mode-locked laser, which uses SWCNTs, was described in 2003 [157]. Carbon nanotubes are an allotropic form of carbon with a cylindrical nanostructure. The carbon nanotubes can be briefly described as a monatomic layer of carbon atoms, known as graphene, rolled into a cylinder. Carbon nanotubes can be either single-walled or multi-walled, consisting of several concentric graphene layers. The cylinder diameter ranges in the nanometer range, and the length is a few micrometers.

Carbon nanotubes can exhibit the properties of a semiconductor, a semimetal, and even a metal. Metal carbon nanotubes exhibit outstanding metallic properties, have 1000 times higher electrical conductivity than copper [158], thermal conductivity is ten times higher than that of copper [159], and tensile strength is 100 times higher than that of stainless steel [160]. The ability to exhibit the properties of various materials depends on the chirality of the nanotubes, which in turn is characterized by the chirality vector *Ch*. There are a vast number of possible combinations of twisting graphene into a carbon nanotube. There are three shapes: achiral armchair (two sides of each hexagon are oriented perpendicular to the carbon nanotube axis), achiral zigzag (two sides of each hexagon are oriented parallel to the carbon nanotube axis), and chiral or helical (each side of the hexagon is located to axis of the carbon nanotube at an angle different from 0 and 90°).

For applications as saturable absorbers, the optical properties of carbon nanotubes are essential. The bandgap and, consequently, the wavelength of the absorption peaks of semiconductor nanotubes depend on the diameter of the nanotubes. Typically, the nanotube's diameter ranges from 0.7 to 1.5 nm, which corresponds to a bandgap from 1.2 to 0.6 eV. The bandgap in this range corresponds to the energies of radiation photons with wavelengths from 1 to 2 μm.

It is necessary to produce nanotubes with a specific diameter to operate at certain wavelengths. However, to date, no process for the production of nanotubes can provide a selective production of nanotubes with the same diameter and chirality. A sample of nanotubes is always a mixture of semiconducting and metallic nanotubes with different chiralities and diameters. By changing the conditions and methods of manufacturing nanotubes, one can only change the number of nanotubes with specific parameters. This feature determines the broad spectral range of nanotube operation as a SA in passively mode-locked lasers.

Basically, during the production of nanotubes, it turns out that 2/3 of the nanotubes are semiconducting and 1/3 exhibits metallic properties. In carbon nanotubes, two mechanisms of recovery from an excited state are observed. The first slow mechanism is associated with the transition of charge carriers from the conduction band to the valence band, and its duration is about one picosecond. The second fast mechanism is associated with metal nanotubes, which play the role of recombination centers, by analogy with defects in semiconductor saturable absorbers, with a relaxation time of about hundreds of femtoseconds [155,161,162]. The typical relaxation times of single-walled carbon nanotubes for different energies are shown in Figure 15. The paper [163] shows that the relaxation time increases with increasing wavelength in the range from 1.06 to 1.55 μm and becomes shorter at about 2 μm. It should be noted that there is no intraband relaxation in carbon nanotubes [150].

The modulation depth of SWCNTs is an essential parameter for their use in mode-locked lasers. It differs in a wide range and can reach 27% [161]. Carbon nanotubes also have non-saturable losses, which amount to ~13% [161]. The ratio of saturable and non-saturable losses in carbon nanotubes is approximately 1/2 [163]. SWCNTs are often part of the polymer to create easy-to-use films. Non-saturable losses also depend on the optical properties of the polymer. The saturation energy of SWCNTs is several tens of microjoules per square centimeter, depending on the radiation wavelength [164], as in typical semiconductor saturable absorbers. The resistance to optical damage of the carbon tubes themselves is quite high. However, the polymer into which they are embedded also affects this parameter and, in most cases, decreases it. For SWCNTs, the optical resistance threshold was 0.35 J/cm^2 [165]. To date, SAs have appeared that consist only of carbon nanotubes without the use of polymer matrices, such as high-density well-aligned single-walled carbon nanotubes [166].

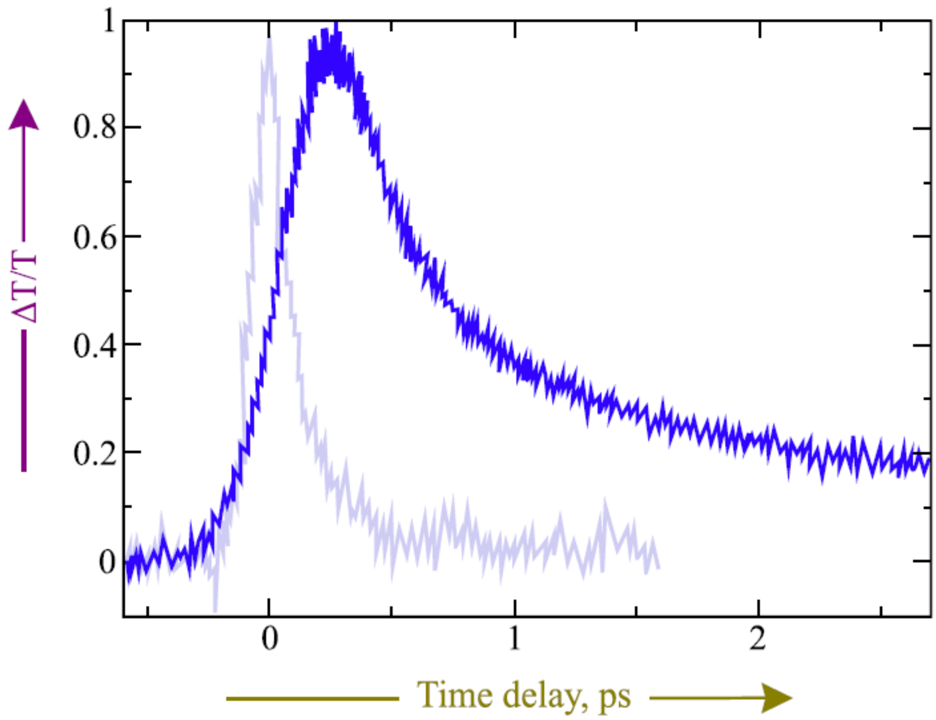

Figure 15. Typical relaxation times of single-walled carbon nanotubes: black color shows relaxation time for 0.8 eV energy and gray color shows relaxation time for 1.47 eV energy.

The most common method for the synthesis of carbon nanotubes is the electric arc method. If evaporating a graphite rod (anode) in an electric arc, a hard carbon build-up is formed on the opposite electrode (cathode), which contains carbon nanotubes. The main problem with this method was low productivity until 1995 [167]. It was proposed to add small amounts of nickel and cobalt to graphite, which increased the yield to 90%. Graphene layers [168] can also be used as a saturable absorber, and lasing can be obtained in mode-locked lasers [169]. The advantage of using graphene is that non-saturable losses are lower than those of carbon nanotubes. However, its widespread use is limited by a minimal modulation depth, which is $\sim 1\%$.

SWCNTs can be used in various laser schemes, both in solid-state lasers and fiber lasers. At present, the most common modules with nanotubes as a saturable absorber incorporating nanotubes (SAINT), which are used in passively mode-locked lasers, are transmission (T-SAINT), reflective (R-SAINT), and fiber (F-SAINT) types. These types of modules are shown in Figure 16.

The duration of pulses in an erbium fiber laser with SWCNTs can be tens of femtoseconds. The first work in which the pulse duration was less than 100 fs appeared in 2012 [170]. A pulse with a duration of 74 fs and a radiation spectrum width of 63 nm was obtained. At present, the shortest pulse duration using SWCNTs is 66 fs with a radiation spectrum width of 54 nm [171]. These results were obtained in an erbium-doped ring-cavity fiber scheme with a positive GVD value. As shown in [48] and [172], the use of SWCNTs in fiber lasers can have a positive effect on the noise characteristics of a fiber laser, i.e., reduce jitter and RIN. Thus, in these works, the value of the temporal jitter was 29.1 fs and 490 as, respectively, and these schemes are shown in Figure 17. It should be noted that the ease of fabrication of nano-tubes contributes to the greater variability of the obtained SA, which in turn leads to the possibility of the better optimization of the intracavity insertion loss and, accordingly, to a more stable generation.

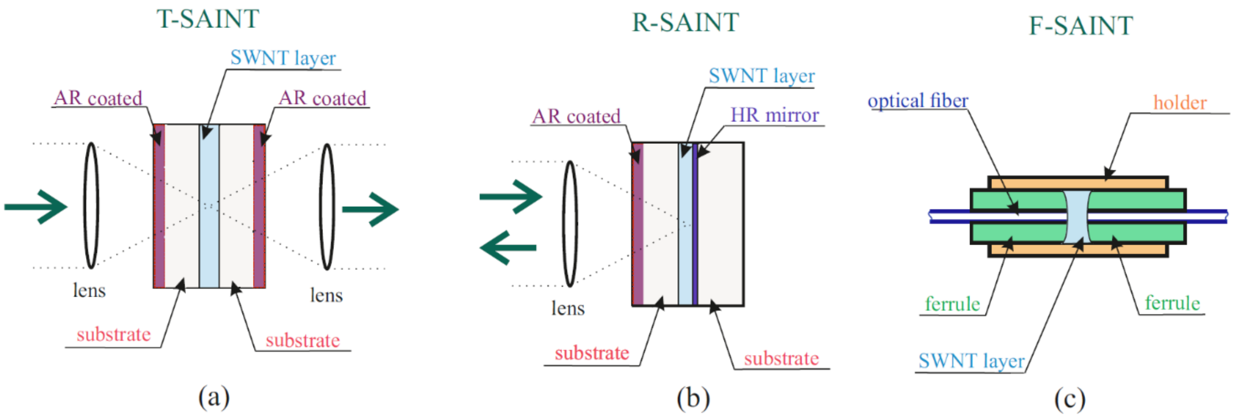

Figure 16. Modules with nanotubes as a saturable absorber: (**a**) transmissive (T-SAINT), (**b**) reflective (R-SAINT), and (**c**) fiber (F-SAINT).

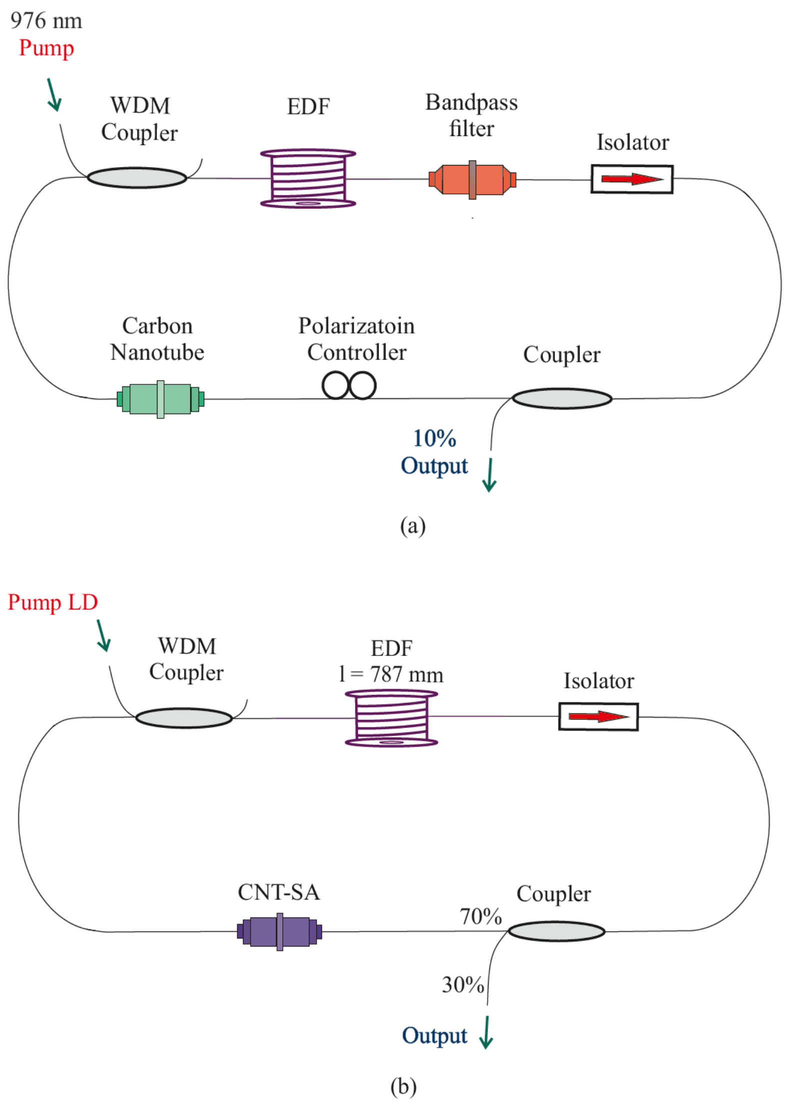

Figure 17. Schemes of fiber lasers using SWCNTs: (**a**) a ring fiber laser with 29.1 femtosecond jitter and (**b**) fiber laser ring circuit with 490 attosecond jitter.

Based on the analysis performed, it can be concluded that SWCNTs are an excellent alternative to a semiconductor saturable absorber. Based on the analysis of the results of the studies [173–175], as well as [48,172], it can be assumed that the use of SWCNTs as an SA reduces jitter and RIN in USP lasers, which is the main advantage for use in lasers with increased requirements for the stability of time and amplitude characteristics. An additional advantage of SWCNTs is their high optical stability, a much cheaper and simpler manufacturing process, and a low generation threshold. However, a significant disadvantage of their use is rather large values of non-saturable losses and a relatively long relaxation time, which does not allow obtaining extremely short pulse durations. In this regard, we consider the possibility of using artificial saturable absorbers based on nonlinear polarization rotation to implement the fiber USP lasers with increased requirements for the stability of the temporal and amplitude characteristics of the output radiation.

4.4. Artificial Saturable Absorbers

The schemes of fiber USP lasers resonators with artificial SAs include methods that can also reduce losses for more intense radiation but do not have saturable absorbers. These include an absorber using nonlinear polarization rotation in a fiber [127,128] and a ring fiber mirror with an active [80,129,130] or passive fiber in the ring [132,133].

4.4.1. Nonlinear Evolution of Polarization

The mechanism of operation of the nonlinear evolution of polarization is based on the dependence of the material's refractive index on the intensity of the radiation passing through it. Birefringence is usually observed in anisotropic crystals. Although glass is an isotropic material, the core of an optical fiber exhibits some birefringence due to mechanical stress. When light passes through the fiber core, the radiation undergoes birefringence. So, waves with mutually perpendicular polarizations propagate along with the fiber at different speeds. The addition of these mutually perpendicular waves results in elliptical polarization within the fiber. By changing the mechanical stresses in the fiber, which can be made both during fiber drawing and by mechanical action, it is possible to regulate the amount of birefringence. Since the wave propagation speed depends on the refractive index, which, in turn, according to Kerr's law, depends on the light intensity, the form of elliptical polarization, i.e., its rotation, also depends on the light intensity. The NEP mechanism is based on this dependence.

Self-phase modulation and cross-modulation caused by the dependence of the refractive index on the intensity lead to the rotation of the polarization ellipse. As a result, one can obtain the situation shown in Figure 18, where there is a significant loss for radiation with lower intensity. NEP strongly depends on the linear birefringence value of the fiber core due to the ellipticity [176]. However, a small linear birefringence can be neglected when the cavity length is more significant or comparable to the polarization beat length. The length of the polarization beat is the length at which the polarization state is restored; it can vary from 1 mm (for fibers with high birefringence) to 100 m (for fibers with low birefringence). The typical polarization beat length for a 1.5 μm wavelength is 100 mm, much less than the typical laser cavity length.

Figure 19 shows a typical NEP mode-locked fiber ring laser. After passing through the insulator polarizer, the radiation becomes linearly polarized. Installed directly behind the insulator, the polarization controller, which is two plates between which the optical fiber is clamped, changes polarization from linear to elliptical. The polarization state evolves nonlinearly under the action of self-phase modulation and cross-modulation. Thus, nonlinear effects create a phase shift between orthogonally polarized components during pulse propagation in the resonator. It is possible to create high radiation intensities due to the small diameter of the fiber core. Therefore, high intensity and long fiber length combined make it possible to obtain a significant nonlinear change in the polarization state.

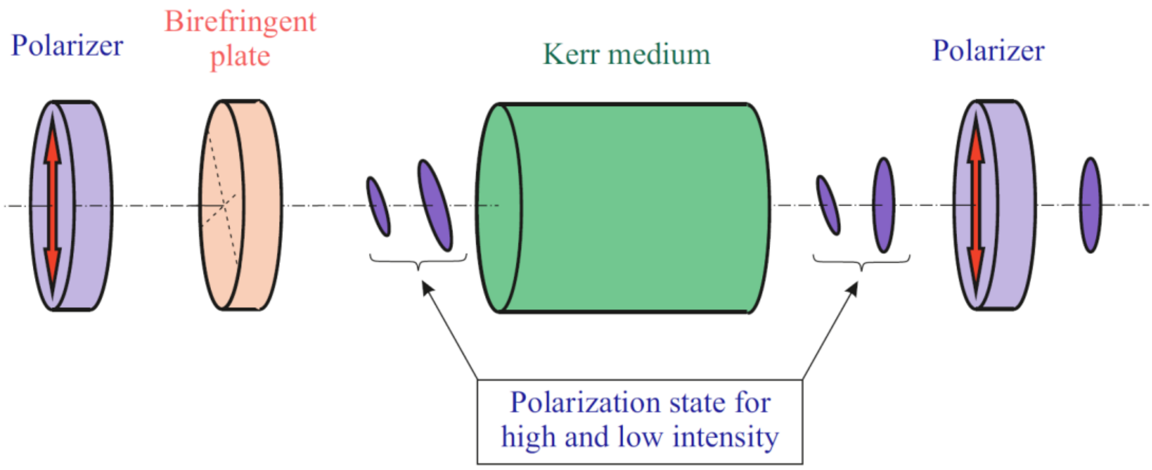

Figure 18. Scheme for obtaining the amplitude self-modulation of radiation in an optical fiber as a result of the nonlinear evolution of polarization.

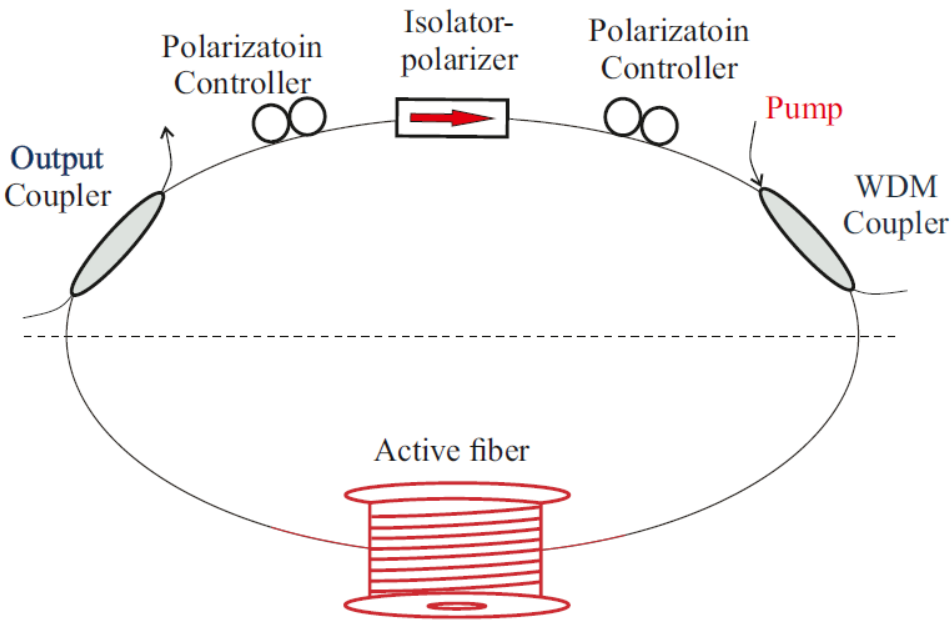

Figure 19. Operating principle of a fiber laser with NEP.

The phase difference of mutually orthogonal modes can be determined by the formula:

$$\Delta\Phi = \frac{\gamma PL}{3} \cdot sin\ 2\alpha \cdot cos\ \varphi, \tag{30}$$

where φ—phase shift provided by the first polarization controller; α—phase shift set by the second polarization controller; P—radiation power; L—resonator length; and γ—fiber nonlinearity parameter.

Nonlinear transmission can be determined by the formula [176]:

$$T(P) = 1 - cos^2\varphi \cdot cos^2\Delta\Phi\left(sin^2\alpha + cos^2\alpha \cdot sin^2\varphi\right) + \frac{1}{2}sin2\Delta\Phi \cdot cos2\alpha \cdot sin2\varphi, \tag{31}$$

and the function will have the form shown in Figure 20 [177].

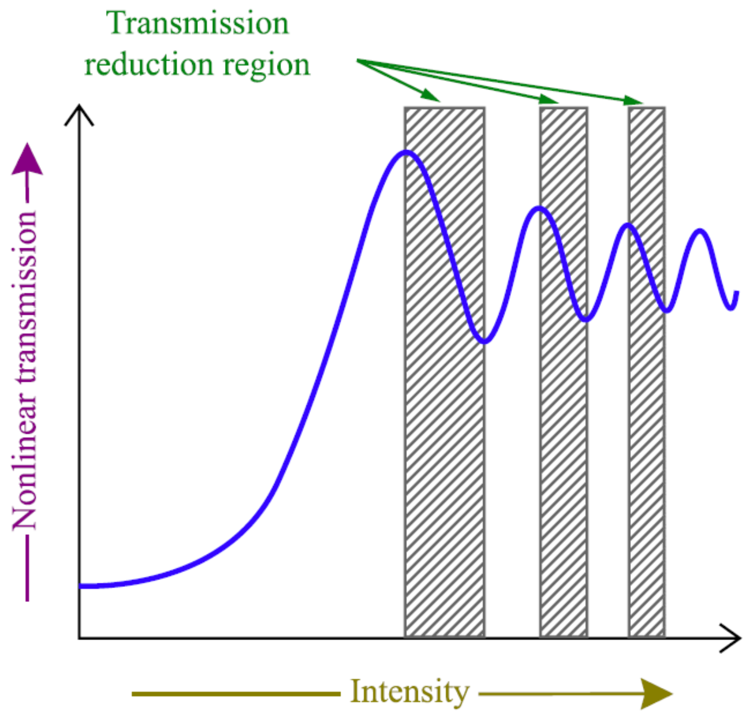

Figure 20. Nonlinear transmission function of an artificial glorifying absorber based on NEP.

The phenomenon of rotation of the polarization ellipse concerning intensity was discovered in materials with Kerr nonlinearity in 1965 [178]. The first laser with mode-locking based on this mechanism was implemented in 1972 [179]. The first passively mode-locked fiber laser based on NEP was shown in 1991 [127], where 70 fs pulses were generated in a neodymium fiber laser. Figure 21 shows the schematic of the laser cavity with the shortest pulse duration in an erbium fiber laser to date, using the NEP mechanism [180]. The pulse duration in this laser was 37.4 fs with a pulse repetition rate of 225 MHz. The disadvantages of this scheme include the presence of non-fiber elements in the scheme, which introduce additional losses and require more accurate alignment.

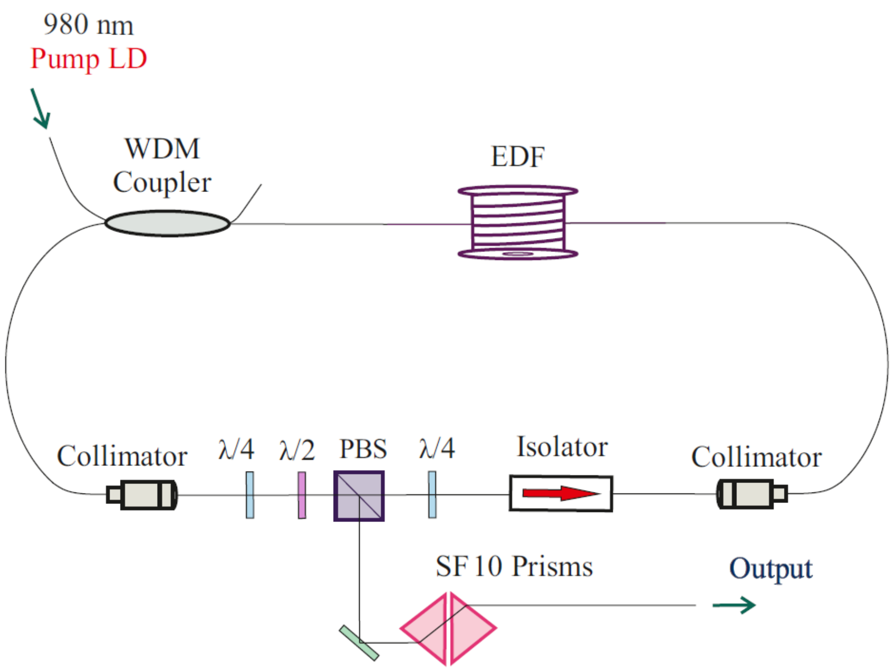

Figure 21. Schematic of an erbium fiber laser with the shortest pulse duration.

The NEP mechanism's main advantage is the theoretical possibility of obtaining pulses up to ten fs duration. Since the Kerr effect has a medium response time of ~ 10 fs [181]. Another important advantage of this mode-locking mechanism is the relatively cheap and widespread element base required for its implementation. However, temperature fluctuations and mechanical stresses can alter birefringence and cause unstable laser operation [182]. Thus, it is necessary to use the temperature stabilized resonator and shorten the fiber length as much as possible. However, in this case, it is necessary to use fibers with high birefringence.

4.4.2. Nonlinear Loop Mirrors

The use of nonlinear loop mirrors as saturable absorbers was proposed in 1988 [132,183]. The principle of operation is based on using a fiber loop mirror in combination with the Kerr effect. The fiber ring mirror is an X-shaped fiber fused coupler with a division factor of 0.5, in which the output fibers are spliced together on one side. A typical fiber mirror layout is shown in Figure 22a.

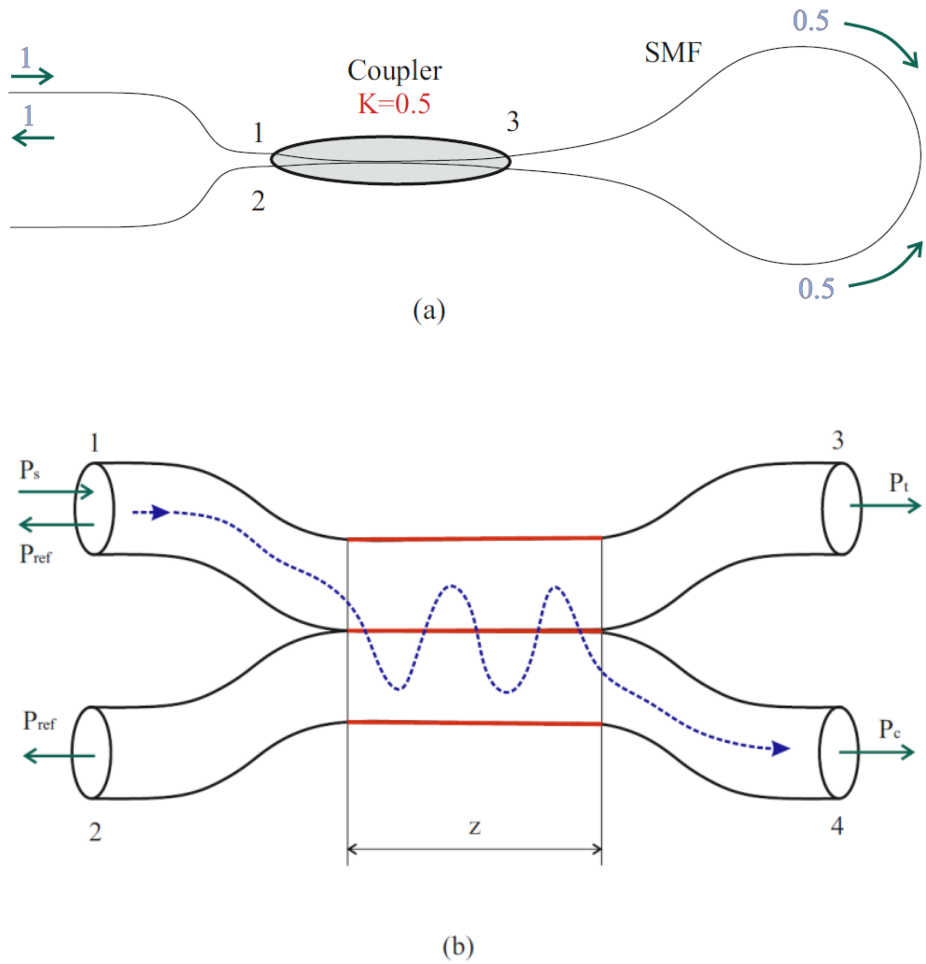

Figure 22. Scheme of a fiber loop mirror and its principle of operation: (**a**) scheme of a fiber loop mirror and (**b**) propagation of radiation in a fiber splitter.

The transfer of radiation in the splitter from one waveguide to another occurs due to the tunneling effect. The process of radiation propagation in the splitter is shown in Figure 22b. The division factor depends on the phase of the propagating radiation or the splitter length [184].

Consider the principle of operation of a conventional fiber loop mirror shown in Figure 22a in the ideal case. Half of the radiation entering the input channel 1 passes clockwise in the loop, and the other half counterclockwise. The radiation in the splitter, passing from one waveguide to another (counterclockwise), receives a phase shift of $\pi/2$ relative to the radiation propagating further along with the input fiber (clockwise). After passing through the loop, the counterclockwise radiation at output 2 will have a phase shift of π relative to the clockwise radiation. As a result of the interference, no radiation will be observed at output 2, and all radiation will be directed to the input fiber 1. In reality, complete reflection from such a mirror cannot be obtained due to losses in the fiber, losses in the splitter, birefringence, and the impossibility of obtaining an accurate division factor of 0.5. If a polarization controller is introduced into a circular fiber mirror, it can be used to introduce a phase difference ϕ, thereby changing the reflection coefficient of the mirror.

The nonlinear loop fiber mirror is realized using a splitter with a division ratio $\alpha \neq 0.5$ and a polarization controller. The radiation is divided into two parts in the splitter with different intensities. In turn, due to the Kerr effect, radiation with a higher intensity receives a larger phase incursion, which depends on the radiation intensity $|E|^2$, the length of the fiber mirror loop L and the nonlinearity coefficient γ. It should be noted that radiation with a lower intensity receives a phase incursion, but less. As a result, the phase difference between radiations propagating in different directions, obtained under the influence of the Kerr effect, is determined by the equation:

$$\delta\theta = (1 - 2\alpha)\frac{2\pi\gamma|E|^2 L}{\lambda} \tag{32}$$

The reflection coefficient of a nonlinear loop mirror can be determined by the equation [133]:

$$R = 2\alpha(1 - \alpha)[1 + \cos(\delta\theta + \varphi)] \tag{33}$$

As can be seen from Equations (32) and (33), the maximum reflection will be when $\delta\theta + \varphi = 2\pi m$, where m is an integer. Since $\delta\theta$ depends on the intensity, the reflection coefficient also depends on the intensity. Therefore, it works as a saturable absorber. The disadvantage of this scheme is that it is impossible to obtain a reflection coefficient equal to 1 because this is only possible when using a splitter with a division ratio $\alpha \neq 0.5$. This contradicts the condition for the formation of the phase incursion. Therefore, a nonlinear loop mirror is more often used in the transmission mode, i.e., all radiation goes to port 2 of Figure 22a. This happens when the phase ratio is $\delta\theta + \varphi = 2\pi m + \pi$, where m is an integer. The scheme of a laser in which the nonlinear loop mirror operates in the transmission mode is shown in Figure 23a. The pulse duration in this scheme was 300 fs at a wavelength of 1060 nm [185]. There are also works where this mechanism has been implemented in a cavity with PM fibers [186]. The dependence of the transmission coefficient of the annular mirror in the transmission mode on the input power for different division factors α is shown in Figure 23b [132].

From Figure 23b, it can be seen that the division ratio α affects the modulation depth, and the most excellent modulation depth is observed when α is close to 0.5. However, at values close to 0.5, the nonlinear loop mirror ceases to work as a saturable absorber due to the absence of a phase difference between the radiations passing in different directions. The following stage in developing a nonlinear loop mirror was the nonlinear amplifying loop mirror (NALM) [129]. One of the first schemes for using this mechanism is shown in Figure 24a. This is a figure-eight scheme with a pulse duration of 2 ps [80].

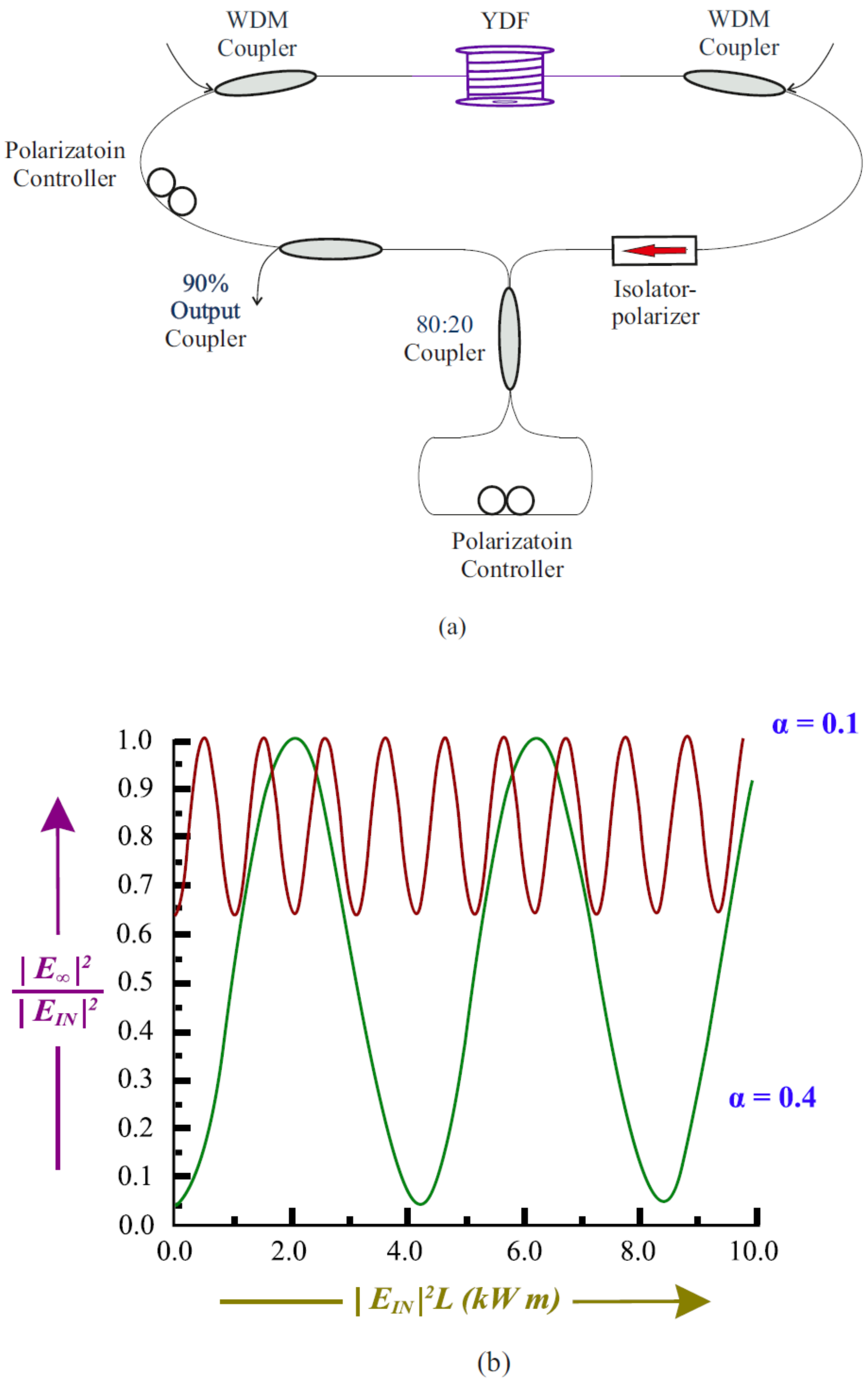

Figure 23. Layout of a laser with a nonlinear loop mirror in the transmission mode and the dependence of the transmittance of the loop mirror: (**a**) layout of a laser with a nonlinear loop mirror in the transmission mode and (**b**) the dependence of the transmittance of the loop mirror in the transmission mode on the input power for different division coefficients α.

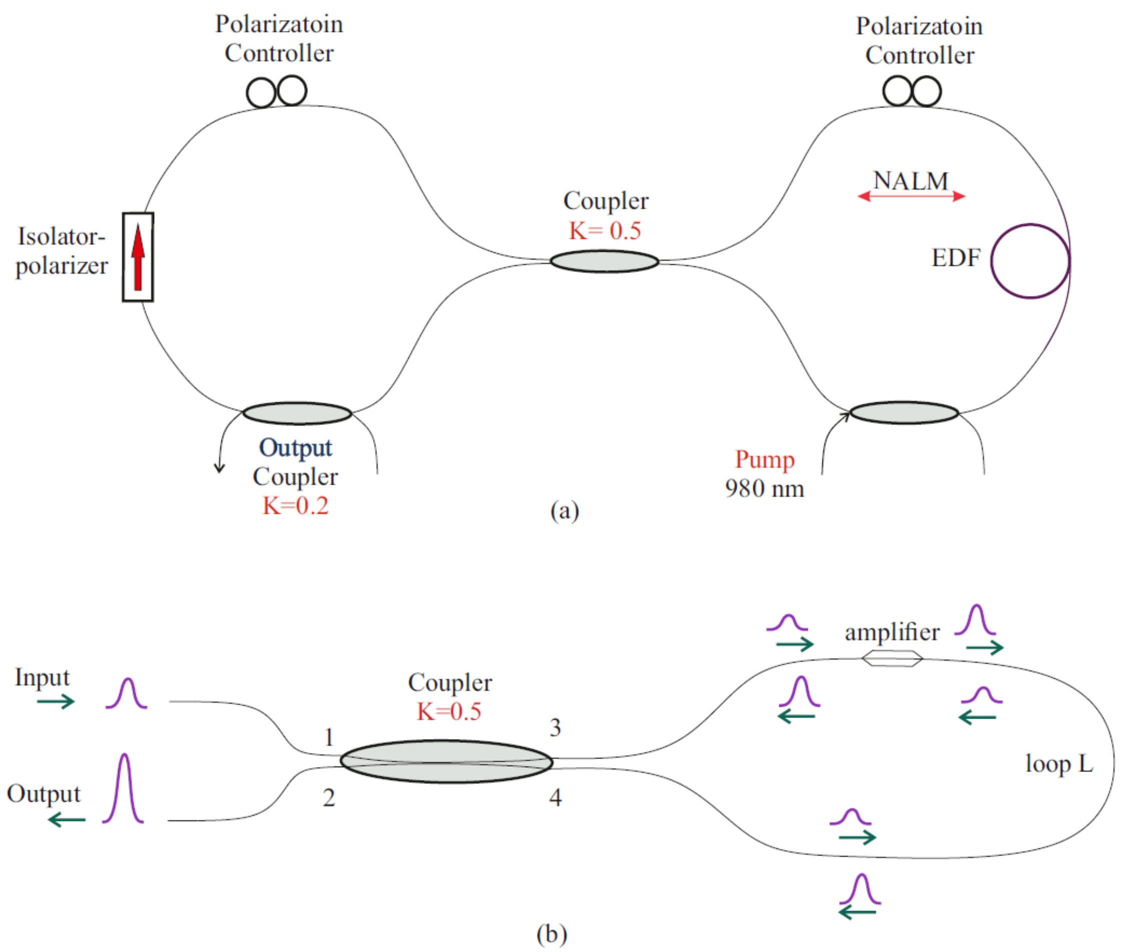

Figure 24. Layout of a laser using a nonlinear amplifying loop mirror and the scheme of its operation: (**a**) layout of a laser with a nonlinear amplifying loop mirror in the transmission mode and (**b**) a diagram of the operation of a nonlinear amplifying loop mirror.

The principle of operation of a nonlinear amplifying loop mirror is also based on the Kerr effect. However, unlike a conventional nonlinear loop mirror, a different phase incursion is provided by introducing an amplifying fiber into the scheme located asymmetrically concerning the splitter. The scheme of the nonlinear amplifying mirror is shown in Figure 24b. The radiation entering the splitter is divided equally and spreads in both clockwise and counterclockwise directions. Clockwise passing radiation is first amplified with a gain of g, and after that, propagates along with the fiber. The equation determines the phase incursion for radiation propagating clockwise:

$$\varphi_{\circlearrowright} = \frac{2\pi\gamma|E|^2 Lg}{\lambda} \tag{34}$$

For radiation that propagates counterclockwise, the phase incursion $\varphi_{\circlearrowleft}$ is determined by the equation:

$$\varphi_{\circlearrowleft} = \frac{2\pi\gamma|E|^2 Lg}{\lambda} \tag{35}$$

Since this radiation is amplified after passing through almost the entire mirror loop, the amplification is not taken into account. Then, the phase difference $\delta\varphi$ between the radiations propagating in both directions is determined by the equation:

$$\delta\varphi = (1-g)\frac{2\pi\gamma|E|^2 Lg}{\lambda} \tag{36}$$

The polarization controller introduces a phase shift φ for emissions traveling in both directions. As a result, the reflection coefficient of the nonlinear amplifying loop mirror can be found by Equation (33) substituting the division coefficient $\alpha = 0.5$. In the nonlinear amplifying loop mirror scheme, splitters with different division ratios can be used to increase the phase difference. However, the modulation depth and reflection coefficient will not be maximized. The use of this mechanism turned out to be very productive, and already in 1993, using a nonlinear amplifying mirror, pulse durations of about 100 fs were obtained [96,187].

Unfortunately, the authors of the cited papers did not provide data on the stability of USP generation modes in schemes with nonlinear fiber mirrors. However, in the theoretical study in [188], it was shown that in such systems, mode-locking pulses are generated due to the modulation instability of stationary solutions. These asymmetric impulses always coexist with a stable solution. Therefore, they can be considered as solitons of the temporal cavity, which have similar properties to the localized light structures observed in bistable spatially extended systems, which indicates a high potential stability, provided that intracavity losses are properly optimized.

5. Hybrid Mode-Locking

The use of saturable absorbers based on NEP has several advantages, which include: the minimum response time of the medium, which makes it possible to obtain pulse durations of tens of femtoseconds; the presence of minimal non-saturable losses; and the absence of the need to purchase additional, expensive elements. However, the use of this type of saturable absorbers also has some disadvantages. Their main disadvantage is the dependence on the medium nonlinearity, which requires long resonators or high pump power. These features negatively affect the stability of the output characteristics of the radiation. Conventional and artificial saturable absorbers have several compensating disadvantages. We consider the possibility of using these two types of saturable absorbers in one cavity to improve the stability of the temporal and amplitude characteristics of the output radiation.

Two saturable absorbers of different types are used simultaneously in the fiber USP lasers with hybrid mode-locking. These schemes combine a natural saturable absorber, SWCNTs or a semiconductor saturable mirror, and an artificial one based on an NEP or a nonlinear loop mirror. This combination is due to the more straightforward implementation of the self-triggering mode-locking. As described above, artificial saturable absorbers have a higher potential for obtaining a minimum duration since they have a response time of the order of ~5–10 fs. However, it is challenging to realize the self-triggering mode since the intensity of the fluctuation peaks is often insufficient to trigger the mode-locking. This is not an obstacle for natural saturable absorbers. Even small fluctuation peaks will initiate mode-locking, but the disadvantage of natural SAs is the relatively long relaxation time, up to hundreds of femtoseconds. Thus, combining two different saturable absorbers in one scheme makes it possible to obtain a short pulse duration, self-triggering with low pump energy, and stable lasing.

The resonator scheme, which includes carbon nanotubes and the NEP mechanism, is shown in Figure 25a [189]. In this scheme, the pulse duration was sub-200 fs, and the RIN value did not exceed -135.4 dBc/Hz (30 Hz–1000 kHz) at a repetition rate of 42.2 MHz with an SNR of ~64 dB (at a resolution of ~300 Hz). Note that the standard deviation of the average output power is no more than 0.06% RMS for 3 h of measurements. Figure 25b shows a diagram of a cavity using a semiconductor saturable absorber and NEP [190]. The pulse duration reached 41.9 fs in this case. A laser cavity using a semiconductor saturable mirror and a nonlinear gain ring mirror is shown in Figure 25c [191]. The pulse duration in this scheme was 170 fs, but it should be noted that this scheme used a system for stabilizing the cavity length. There are all-fiber schemes for implementing such a hybrid mode-locking mechanism [192]. Figure 25d shows a resonator scheme that uses carbon nanotubes and a nonlinear amplifying ring mirror mechanism [193]. The pulse duration in this cavity configuration was 230 fs. Together with artificial saturable absorbers, one can use slow saturable absorbers as a semiconductor saturable mirror or carbon nanotubes [194,195]. Since the leading work on the formation of the pulse duration is still performed by fast mechanisms based on NEP.

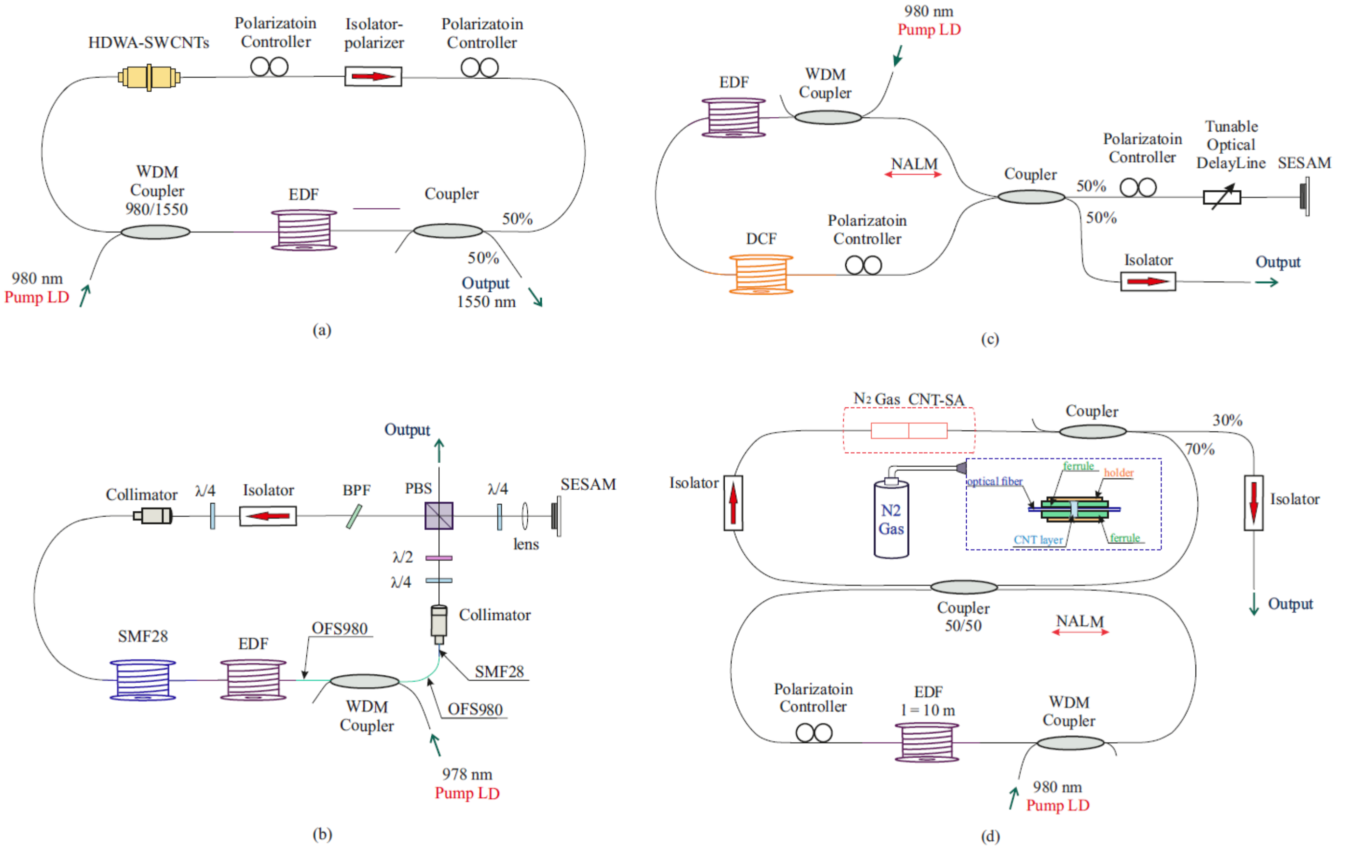

Figure 25. Schemes of fiber lasers with hybrid mode locking: (**a**) using carbon nanotubes and nonlinear polarization rotation; (**b**) using a semiconductor saturable absorber and nonlinear polarization rotation; (**c**) using a semiconductor saturable absorber and a nonlinear amplifying loop mirror; and (**d**) using carbon nanotubes and a nonlinear amplifying loop mirror.

The analysis showed that the use of hybrid mode-locking in fiber lasers makes it possible to compensate for the drawbacks of different types of saturable absorbers and obtain several advantages over schemes in which only one type of saturable absorbers is used. Hybrid mode-locked fiber lasers have the shortest pulse duration, a low lasing threshold, increased output radiation stability, and self-triggering. However, the use of two saturable absorbers in the resonator scheme increases the complexity of the scheme.

6. Conclusions

This review considered the parameters of four primary generation modes in fiber USP lasers cavities, such as solitons, stretched pulse generation, similaritons, and dissipative solitons. The main features of the implementation of these modes in various schemes of fiber resonators are shown. The paper presented the typical calculations of the energy and pulse duration for these generation modes for various schemes for the implementation of resonators. The potential of these modes for use in schemes with increased requirements for the stability of the output characteristics of USP laser radiation was analyzed. The analysis of external and internal factors affecting the stability of the output characteristics of radiation was carried out, depending on the used generation mode and the resonator scheme. Mechanisms of passive mode-locking were described using natural saturable absorbers, including SESAM and carbon nanostructures, and artificial ones based on nonlinear effects in optical fiber. Their features and the potential of their application in the schemes of USP lasers fiber resonators for increasing the stability of the output characteristics of radiation were considered. The primary schemes of resonators used in fiber USP lasers, both in the all-fiber version and open sections, were analyzed. The main features of these schemes were described, and their advantages and disadvantages were provided. The paper described the advantages and disadvantages of using hybrid mode-locking in USP fiber lasers, which combines natural and artificial saturable absorbers.

Applications in which the stability of USP laser is important are constantly expanding. At the same time, the requirements for the characteristics of such lasers increase every year. It can be seen that work on improving the stability parameters in USP laser is actively continuing at present. Almost every year, new methods for improving the stability of output characteristics, as well as new methods for measuring and controlling them, appear. There are studies of new saturable absorbers and generation modes, as well as various laser schemes, in which they try to obtain the best values for the stability of radiation characteristics.

Author Contributions: Conceptualization, S.G.S., D.A.D., L.K.D. and V.E.K.; methodology, S.G.S., D.A.D., L.K.D. and V.E.K.; software: I.O.O., U.S.L. and A.I.; validation: D.A.D.; formal analysis: I.O.O. and A.I.; investigation: I.O.O., U.S.L. and A.I.; data curation: I.O.O., U.S.L. and A.I.; writing—original draft preparation, S.G.S., I.O.O., D.A.D., A.I., L.K.D. and V.E.K.; writing—review and editing, S.G.S., I.O.O., L.K.D. and V.E.K.; visualization, U.S.L.; supervision, S.G.S.; project administration, S.G.S. All authors have read and agreed to the published version of the manuscript.

Funding: This research was funded by Bauman Moscow State Technical University.

Conflicts of Interest: The authors declare no conflict of interest.

References

1. Sugioka, K.; Cheng, Y. Ultrafast lasers—Reliable tools for advanced materials processing. *Light Sci. Appl.* **2014**, *3*, e149. [CrossRef]
2. Coddington, I.; Newbury, N.; Swann, W. Dual-comb spectroscopy. *Optica* **2016**, *3*, 414–426. [CrossRef] [PubMed]
3. Schliesser, A.; Picqué, N.; Hänsch, T.W. Mid-infrared frequency combs. *Nat. Photonics* **2012**, *6*, 440–449. [CrossRef]
4. Kim, J.; Song, Y. Ultralow-noise mode-locked fiber lasers and frequency combs: Principles, status, and applications. *Adv. Opt. Photonics* **2016**, *8*, 465–540. [CrossRef]
5. Gong, Q.; Zhao, W. Ultrafast Science to Capture Ultrafast Motions. *Ultrafast Sci.* **2021**, *2021*, 9765859. [CrossRef]
6. McCumber, D.E. Intensity Fluctuations in the Output of cw Laser Oscillators. I. *Phys. Rev.* **1966**, *141*, 306–322. [CrossRef]
7. Haus, H.; Mecozzi, A. Noise of mode-locked lasers. *IEEE J. Quantum Electron.* **1993**, *29*, 983–996. [CrossRef]
8. Paschotta, R. Noise of mode-locked lasers (Part I): Numerical model. *Appl. Phys. A* **2004**, *79*, 153–162. [CrossRef]
9. Udem, T.; Holzwarth, R.; Hänsch, T.W. Optical frequency metrology. *Nature* **2002**, *416*, 233–237. [CrossRef]
10. Washburn, B.R.; Diddams, S.; Newbury, N.; Nicholson, J.W.; Yan, M.F.; Jørgensen, C.G. Phase-locked, erbium-fiber-laser-based frequency comb in the near infrared. *Opt. Lett.* **2004**, *29*, 250–252. [CrossRef]
11. Gubin, M.; Kireev, A.N.; Tausenev, A.; Konyashchenko, A.V.; Kryukov, P.G.; Tyurikov, D.A.; Shelkovikov, A.S. Femtosecond Er3+ fiber laser for application in an optical clock. *Laser Phys.* **2007**, *17*, 1286–1291. [CrossRef]
12. Zaytsev, K.I.; Gavdush, A.A.; Karasik, V.E.; Alekhnovich, V.I.; Nosov, P.A.; Lazarev, V.A.; Reshetov, I.V.; Yurchenko, S.O. Accuracy of sample material parameters reconstruction using terahertz pulsed spectroscopy. *J. Appl. Phys.* **2014**, *115*, 193105. [CrossRef]
13. Eckstein, J.N.; Ferguson, A.I.; Hänsch, T.W. High-Resolution Two-Photon Spectroscopy with Picosecond Light Pulses. *Phys. Rev. Lett.* **1978**, *40*, 847–850. [CrossRef]
14. Baklanov, Y.V.; Chebotayev, V.P. Narrow resonances of two-photon absorption of super-narrow pulses in a gas. *Appl. Phys. A* **1977**, *12*, 97–99. [CrossRef]
15. Eckstein, J.N. *High Resolution Spectroscopy Using Multiple Coherent Interactions*; Stanford University: Stanford, CA, USA, 1978.
16. Picqué, N.; Hänsch, T.W. Frequency comb spectroscopy. *Nat. Photonics* **2019**, *13*, 146–157. [CrossRef]
17. Gerry, C.; Knight, P. *Introductory Quantum Optics*; Cambridge University Press: Cambridge, UK, 2004. [CrossRef]
18. Washburn, B.R.; Swann, W.C.; Newbury, N. Response dynamics of the frequency comb output from a femtosecond fiber laser. *Opt. Express* **2005**, *13*, 10622–10633. [CrossRef]
19. Paschotta, R.; Telle, H.; Keller, U. Noise of Solid-State Lasers. In *Optical Science and Engineering*; CRC Press: Boca Raton, FL, USA, 2006; pp. 473–510. [CrossRef]
20. Ozeki, Y. Molecular vibrational imaging by stimulated Raman scattering microscopy: Principles and applications [Invited]. *Chin. Opt. Lett.* **2020**, *18*, 121702. [CrossRef]
21. Cheng, J.-X.; Xie, X.S. Vibrational spectroscopic imaging of living systems: An emerging platform for biology and medicine. *Science* **2015**, *350*, aaa8870. [CrossRef]

22. Valley, G.C. Photonic analog-to-digital converters. *Opt. Express* **2007**, *15*, 1955–1982. [CrossRef]
23. Taylor, H. An optical analog-to-digital converter—Design and analysis. *IEEE J. Quantum Electron.* **1979**, *15*, 210–216. [CrossRef]
24. Steinke, M.; Tunnermann, H.; Kuhn, V.; Theeg, T.; Karow, M.; de Varona, O.; Jahn, P.; Booker, P.; Neumann, J.; Wesels, P.; et al. Single-Frequency Fiber Amplifiers for Next-Generation Gravitational Wave Detectors. *IEEE J. Sel. Top. Quantum Electron.* **2017**, *24*, 3100613. [CrossRef]
25. Mayer, A.S.; Grosinger, W.; Fellinger, J.; Winkler, G.; Perner, L.W.; Droste, S.; Salman, S.H.; Li, C.; Heyl, C.M.; Hartl, I.; et al. Flexible all-PM NALM Yb:fiber laser design for frequency comb applications: Operation regimes and their noise properties. *Opt. Express* **2020**, *28*, 18946. [CrossRef]
26. Liu, G.; Jiang, X.; Wang, A.; Chang, G.; Kaertner, F.; Zhang, Z. Robust 700 MHz mode-locked Yb:fiber laser with a biased nonlinear amplifying loop mirror. *Opt. Express* **2018**, *26*, 26003–26008. [CrossRef]
27. Chen, W.; Song, Y.; Jung, K.; Hu, M.; Wang, C.; Kim, J. Few-femtosecond timing jitter from a picosecond all-polarization-maintaining Yb-fiber laser. *Opt. Express* **2016**, *24*, 1347–1357. [CrossRef]
28. Gierschke, P.; Jauregui, C.; Gottschall, T.; Limpert, J. Relative amplitude noise transfer function of an Yb^{3+}-doped fiber amplifier chain. *Opt. Express* **2019**, *27*, 17041–17050. [CrossRef]
29. Cheng, H.; Wang, W.; Zhou, Y.; Qiao, T.; Lin, W.; Guo, Y.; Xu, S.; Yang, Z. High-repetition-rate ultrafast fiber lasers. *Opt. Express* **2018**, *26*, 16411–16421. [CrossRef]
30. Qin, P.; Song, Y.; Kim, H.; Shin, J.; Kwon, D.; Hu, M.; Wang, C.; Kim, J. Reduction of timing jitter and intensity noise in normal-dispersion passively mode-locked fiber lasers by narrow band-pass filtering. *Opt. Express* **2014**, *22*, 28276–28283. [CrossRef]
31. Wang, Y.; Tian, H.; Hou, D.; Meng, F.; Ma, Y.; Xu, H.; Kärtner, F.X.; Song, Y.; Zhang, Z. Timing jitter reduction through relative intensity noise suppression in high-repetition-rate mode-locked fiber lasers. *Opt. Express* **2019**, *27*, 11273–11280. [CrossRef]
32. Ma, Y.; Salman, H.S.; Li, C.; Mahnke, C.; Hua, Y.; Droste, S.; Fellinger, J.; Mayer, A.S.; Heckl, O.; Heyl, C.; et al. Compact, all-PM fiber integrated and alignment-free ultrafast Yb:fiber NALM laser with sub-femtosecond timing jitter. *J. Lightwave Technol.* **2021**, *39*, 4431–4438. [CrossRef]
33. Li, Y.; Kuse, N.; Rolland, A.; Stepanenko, Y.; Radzewicz, C.; Fermann, M.E. Low noise, self-referenced all polarization maintaining Ytterbium fiber laser frequency comb. *Opt. Express* **2017**, *25*, 18017–18023. [CrossRef]
34. Vicentini, E.; Wang, Y.; Gatti, D.; Gambetta, A.; Laporta, P.; Galzerano, G.; Curtis, K.; McEwan, K.; Howle, C.R.; Coluccelli, N. Nonlinear pulse compression to 22 fs at 15.6 μJ by an all-solid-state multipass approach. *Opt. Express* **2020**, *28*, 4541–4549. [CrossRef] [PubMed]
35. Zhou, J.; Pan, W.; Fu, X.; Zhang, L.; Feng, Y. Environmentally-stable 50-fs pulse generation directly from an Er:fiber oscillator. *Opt. Fiber Technol.* **2019**, *52*, 101963. [CrossRef]
36. Audier, X.; Heuke, S.; Volz, P.; Rimke, I.; Rigneault, H. Noise in stimulated Raman scattering measurement: From basics to practice. *APL Photonics* **2020**, *5*, 011101. [CrossRef]
37. Dai, G.; Katoh, K.; Ozeki, Y. Reduction of excess intensity noise of picosecond Yb soliton fiber lasers in a >10-mW power regime. *Opt. Express* **2021**, *29*, 11702–11711. [CrossRef]
38. Cranch, G.A.; Kirkendall, C.K. Emission properties of a passively mode-locked fiber laser for time division multiplexing of fiber Bragg grating array applications. In Proceedings of the 17th International Conference on Optical Fibre Sensors, Bruges, Belgium, 23–27 May 2005; pp. 980–983. [CrossRef]
39. Newbury, N.R.; Swann, W.C. Low-noise fiber-laser frequency combs. *JOSA B* **2007**, *24*, 1756–1770. [CrossRef]
40. Budunoğlu, I.L.; Ülgüdür, C.; Oktem, B.; Ilday, F.Ö. Intensity noise of mode-locked fiber lasers. *Opt. Lett.* **2009**, *34*, 2516–2518. [CrossRef]
41. Wang, H.-B.; Han, H.-N.; Zhang, Z.-Y.; Shao, X.-D.; Zhu, J.-F.; Wei, Z.-Y. An Yb-fiber frequency comb phase-locked to microwave standard and optical reference. *Chin. Phys. B* **2020**, *29*, 030601. [CrossRef]
42. Nishizawa, N.; Suga, H.; Yamanaka, M. Investigation of dispersion-managed, polarization-maintaining Er-doped figure-nine ultrashort-pulse fiber laser. *Opt. Express* **2019**, *27*, 19218–19232. [CrossRef]
43. Kim, C.; Kim, D.; Cheong, Y.; Kwon, D.; Choi, S.Y.; Jeong, H.; Cha, S.J.; Lee, J.-W.; Yeom, D.-I.; Rotermund, F.; et al. 300-MHz-repetition-rate, all-fiber, femtosecond laser mode-locked by planar lightwave circuit-based saturable absorber. *Opt. Express* **2015**, *23*, 26234–26242. [CrossRef]
44. Nugent-Glandorf, L.; Johnson, T.A.; Kobayashi, Y.; Diddams, S.A. Impact of dispersion on amplitude and frequency noise in a Yb-fiber laser comb. *Opt. Lett.* **2011**, *36*, 1578–1580. [CrossRef]
45. Kim, D.; Zhang, S.; Kwon, D.; Liao, R.; Cui, Y.; Zhang, Z.; Song, Y.; Kim, J. Intensity noise suppression in mode-locked fiber lasers by double optical bandpass filtering. *Opt. Lett.* **2017**, *42*, 4095–4098. [CrossRef] [PubMed]
46. Oktem, B.; Ulgudur, C.; Ilday, F.Ö. Soliton-similariton fibre laser. *Nat. Photonics* **2010**, *4*, 307–311. [CrossRef]
47. Jauregui, C.; Müller, M.; Kienel, M.; Emaury, F.; Saraceno, C.J.; Limpert, J.; Keller, U.; Tünnermann, A. Optimizing the noise characteristics of high-power fiber laser systems. In *Fiber Lasers XIV: Technology and Systems*; SPIE LASE: San Francisco, CA, USA, 2017; Volume 10083, pp. 164–167. [CrossRef]
48. Ouyang, C.; Shum, P.; Wang, H.; Wong, J.H.; Wu, K.; Fu, S.; Li, R.; Kelleher, E.J.R.; Chernov, A.I.; Obraztsova, E.D. Observation of timing jitter reduction induced by spectral filtering in a fiber laser mode locked with a carbon nanotube-based saturable absorber. *Opt. Lett.* **2010**, *35*, 2320–2322. [CrossRef]
49. Paschotta, R. Noise of mode-locked lasers (Part II): Timing jitter and other fluctuations. *Appl. Phys. A* **2004**, *79*, 163–173. [CrossRef]

50. Paschotta, R. Timing jitter and phase noise of mode-locked fiber lasers. *Opt. Express* **2010**, *18*, 5041–5054. [CrossRef]
51. Gordon, J.P.; Haus, H.A. Random walk of coherently amplified solitons in optical fiber transmission. *Opt. Lett.* **1986**, *11*, 665–667. [CrossRef]
52. Fermann, M.E.; Hartl, I. Ultrafast Fiber Laser Technology. *IEEE J. Sel. Top. Quantum Electron.* **2009**, *15*, 191–206. [CrossRef]
53. Shin, J.; Jung, K.; Song, Y.; Kim, J. Characterization and analysis of timing jitter in normal-dispersion mode-locked Er-fiber lasers with intra-cavity filtering. *Opt. Express* **2015**, *23*, 22898–22906. [CrossRef] [PubMed]
54. Fortier, T.; Baumann, E. 20 years of developments in optical frequency comb technology and applications. *Commun. Phys.* **2019**, *2*, 153. [CrossRef]
55. Ho, P.-T. Phase and amplitude fluctuations in a mode-locked laser. *IEEE J. Quantum Electron.* **1985**, *11*, 1806–1813. [CrossRef]
56. Telle, H.; Lipphardt, B.; Stenger, J. Kerr-lens, mode-locked lasers as transfer oscillators for optical frequency measurements. *Appl. Phys. A* **2002**, *74*, 1–6. [CrossRef]
57. Schawlow, A.L.; Townes, C.H. Infrared and Optical Masers. *Phys. Rev.* **1958**, *112*, 1940–1949. [CrossRef]
58. Tian, H.; Song, Y.; Hu, M. Noise Measurement and Reduction in Mode-Locked Lasers: Fundamentals for Low-Noise Optical Frequency Combs. *Appl. Sci.* **2021**, *11*, 7650. [CrossRef]
59. Paschotta, R.; Schlatter, A.; Zeller, S.; Keller, U. Optical phase noise and carrier-envelope offset noise of mode-locked lasers. *Appl. Phys. B* **2006**, *82*, 265–273. [CrossRef]
60. Hänsch, T.W. Nobel Lecture: Passion for precision. *Rev. Mod. Phys.* **2006**, *78*, 1297–1309. [CrossRef]
61. Xu, L.; Hänsch, T.W.; Spielmann, C.; Poppe, A.; Brabec, T.; Krausz, F. Route to phase control of ultrashort light pulses. *Opt. Lett.* **1996**, *21*, 2008–2010. [CrossRef] [PubMed]
62. Telle, H.; Steinmeyer, G.; Dunlop, A.; Stenger, J.; Sutter, D.; Keller, U. Carrier-envelope offset phase control: A novel concept for absolute optical frequency measurement and ultrashort pulse generation. *Appl. Phys. A* **1999**, *69*, 327–332. [CrossRef]
63. Jones, D.J.; Diddams, S.A.; Ranka, J.K.; Stentz, A.; Windeler, R.S.; Hall, J.L.; Cundiff, S.T. Carrier-Envelope Phase Control of Femtosecond Mode-Locked Lasers and Direct Optical Frequency Synthesis. *Science* **2000**, *288*, 635–639. [CrossRef]
64. Peters, W.K.; Jones, T.; Efimov, A.; Pedersoli, E.; Foglia, L.; Mincigrucci, R.; Nikolov, I.; Trebino, R.; Danailov, M.B.; Capotondi, F.; et al. All-optical single-shot complete electric field measurement of extreme ultraviolet free electron laser pulses. *Optica* **2021**, *8*, 545. [CrossRef]
65. Kurucz, M.; Tóth, S.; Flender, R.; Haizer, L.; Kiss, B.; Persielle, B.; Cormier, E. Single-shot CEP drift measurement at arbitrary repetition rate based on dispersive Fourier transform. *Opt. Express* **2019**, *27*, 13387–13399. [CrossRef]
66. Fukahori, S.; Ando, T.; Miura, S.; Kanya, R.; Yamanouchi, K.; Rathje, T.; Paulus, G.G. Determination of the absolute carrier-envelope phase by angle-resolved photoelectron spectra of Ar by intense circularly polarized few-cycle pulses. *Phys. Rev. A* **2017**, *95*, 053410. [CrossRef]
67. Wittmann, T.; Horvath, B.; Helml, W.; Schatzel, M.G.; Gu, X.; Cavalieri, A.L.; Paulus, G.G.; Kienberger, R. Single-shot carrier–envelope phase measurement of few-cycle laser pulses. *Nat. Phys.* **2009**, *5*, 357–362. [CrossRef]
68. Sayler, A.M.; Rathje, T.; Müller, W.; Rühle, K.; Kienberger, R.; Paulus, G.G. Precise, real-time, every-single-shot, carrier-envelope phase measurement of ultrashort laser pulses. *Opt. Lett.* **2010**, *36*, 1–3. [CrossRef] [PubMed]
69. Hoff, D.; Furch, F.J.; Witting, T.; Rühle, K.; Adolph, D.; Sayler, A.M.; Vrakking, M.; Paulus, G.G.; Schulz, C.P. Continuous every-single-shot carrier-envelope phase measurement and control at 100 kHz. *Opt. Lett.* **2018**, *43*, 3850–3853. [CrossRef] [PubMed]
70. Adolph, D.; Möller, M.; Bierbach, J.; Schwab, M.; Sävert, A.; Yeung, M.; Sayler, A.M.; Zepf, M.; Kaluza, M.C.; Paulus, G.G. Real-time, single-shot, carrier-envelope-phase measurement of a multi-terawatt laser. *Appl. Phys. Lett.* **2017**, *110*, 081105. [CrossRef]
71. Johnson, N.G.; Herrwerth, O.; Wirth, A.; De, S.; Ben-Itzhak, I.; Lezius, M.; Bergues, B.; Kling, M.F.; Senftleben, A.; Schröter, C.D.; et al. Single-shot carrier-envelope-phase-tagged ion-momentum imaging of nonsequential double ionization of argon in intense 4-fs laser fields. *Phys. Rev. A* **2011**, *83*, 013412. [CrossRef]
72. Schöffler, M.S.; Xie, X.; Wustelt, P.; Möller, M.; Roither, S.; Kartashov, D.; Sayler, A.M.; Baltuska, A.; Paulus, G.G.; Kitzler, M. Laser-subcycle control of sequential double-ionization dynamics of helium. *Phys. Rev. A* **2016**, *93*, 063421. [CrossRef]
73. Kangaparambil, S.; Hanus, V.; Dorner-Kirchner, M.; He, P.; Larimian, S.; Paulus, G.; Baltuška, A.; Xie, X.; Yamanouchi, K.; He, F.; et al. Generalized Phase Sensitivity of Directional Bond Breaking in the Laser-Molecule Interaction. *Phys. Rev. Lett.* **2020**, *125*, 023202. [CrossRef]
74. Hanus, V.; Kangaparambil, S.; Larimian, S.; Dorner-Kirchner, M.; Xie, X.; Schöffler, M.S.; Paulus, G.G.; Baltuška, A.; Staudte, A.; Kitzler-Zeiler, M. Experimental Separation of Subcycle Ionization Bursts in Strong-Field Double Ionization of H2. *Phys. Rev. Lett.* **2020**, *124*, 103201. [CrossRef] [PubMed]
75. Kim, Y.H.; Ivanov, I.A.; Hwang, S.I.; Kim, K.; Nam, C.H.; Kim, K.T. Attosecond streaking using a rescattered electron in an intense laser field. *Sci. Rep.* **2020**, *10*, 22075. [CrossRef]
76. Hansinger, P.; Töpfer, P.; Dimitrov, N.; Adolph, D.; Hoff, D.; Rathje, T.; Sayler, A.M.; Dreischuh, A.; Paulus, G.G. Refractive index dispersion measurement using carrier-envelope phasemeters. *New J. Phys.* **2017**, *19*, 023040. [CrossRef]
77. Chelkowski, S.; Bandrauk, A.D. Asymmetries in strong-field photoionization by few-cycle laser pulses: Kinetic-energy spectra and semiclassical explanation of the asymmetries of fast and slow electrons. *Phys. Rev. A* **2005**, *71*, 053815. [CrossRef]

78. Möller, M.; Sayler, A.M.; Rathje, T.; Chini, M.; Chang, Z.; Paulus, G.G. Precise, real-time, single-shot carrier-envelope phase measurement in the multi-cycle regime. *Appl. Phys. Lett.* **2011**, *99*, 121108. [CrossRef]
79. Kübel, M.; Betsch, K.J.; Johnson, N.G.; Kleineberg, U.; Moshammer, R.; Ullrich, J.; Paulus, G.G.; Kling, M.F.; Bergues, B. Carrier-envelope-phase tagging in measurements with long acquisition times. *New J. Phys.* **2012**, *14*, 093027. [CrossRef]
80. Duling, I.N. All-fiber ring soliton laser mode locked with a nonlinear mirror. *Opt. Lett.* **1991**, *16*, 539–541. [CrossRef] [PubMed]
81. Tamura, K.; Ippen, E.P.; Haus, H.A. Pulse dynamics in stretched-pulse fiber lasers. *Appl. Phys. Lett.* **1995**, *67*, 158–160. [CrossRef]
82. Ilday, F.; Buckley, J.R.; Clark, W.G.; Wise, F.W. Self-Similar Evolution of Parabolic Pulses in a Laser. *Phys. Rev. Lett.* **2004**, *92*, 213902. [CrossRef] [PubMed]
83. Renninger, W.H.; Chong, A.; Wise, F.W. Dissipative solitons in normal-dispersion fiber lasers. *Phys. Rev. A* **2008**, *77*, 023814. [CrossRef]
84. Haus, H.A. Theory of mode locking with a fast saturable absorber. *J. Appl. Phys.* **1975**, *46*, 3049–3058. [CrossRef]
85. Wise, F.; Chong, A.; Renninger, W. High-energy femtosecond fiber lasers based on pulse propagation at normal dispersion. *Laser Photonics Rev.* **2008**, *2*, 58–73. [CrossRef]
86. Agrawal, G. Chapter 2—Pulse Propagation in Fibers. In *Nonlinear Fiber Optics*, 5th ed.; Agrawal, G., Ed.; Academic Press: Boston, MA, USA, 2013; pp. 27–56. [CrossRef]
87. Kutz, J.N.; Collings, B.C.; Bergman, K.; Tsuda, S.; Cundiff, S.; Knox, W.H.; Holmes, P.; Weinstein, M. Mode-locking pulse dynamics in a fiber laser with a saturable Bragg reflector. *J. Opt. Soc. Am. B* **1997**, *14*, 2681–2690. [CrossRef]
88. Tamura, K.; Nelson, L.E.; Haus, H.A.; Ippen, E.P. Soliton versus nonsoliton operation of fiber ring lasers. *Appl. Phys. Lett.* **1994**, *64*, 149–151. [CrossRef]
89. Kadel, R.; Washburn, B.R. Stretched-pulse and solitonic operation of an all-fiber thulium/holmium-doped fiber laser. *Appl. Opt.* **2015**, *54*, 746–750. [CrossRef]
90. Zabusky, N.J.; Kruskal, M.D. Interaction of "Solitons" in a Collisionless Plasma and the Recurrence of Initial States. *Phys. Rev. Lett.* **1965**, *15*, 240–243. [CrossRef]
91. Zakharov, V.F.; Shabat, A.B. Exact Theory of Two-dimensional Self-focusing and One-dimensional Self-modulation of Wave in Nonlinear Media. *Sov. Phys. JETP* **1972**, *34*, 62.
92. Mollenauer, L.F.; Stolen, R.H.; Gordon, J.P. Experimental Observation of Picosecond Pulse Narrowing and Solitons in Optical Fibers. *Phys. Rev. Lett.* **1980**, *45*, 1095–1098. [CrossRef]
93. Agrawal, G.P. Chapter 5—Optical Solitons. In *Nonlinear Fiber Optics*, 5th ed.; Agrawal, G., Ed.; Academic Press: Boston, MA, USA, 2013; pp. 129–191. [CrossRef]
94. Emplit, P.; Hamaide, J.; Reynaud, F.; Froehly, C.; Barthelemy, A. Picosecond steps and dark pulses through nonlinear single mode fibers. *Opt. Commun.* **1987**, *62*, 374–379. [CrossRef]
95. Kelly, S. Characteristic sideband instability of periodically amplified average soliton. *Electron. Lett.* **1992**, *28*, 806–807. [CrossRef]
96. Dennis, M.L.; Duling, I.N. Role of dispersion in limiting pulse width in fiber lasers. *Appl. Phys. Lett.* **1993**, *62*, 2911–2913. [CrossRef]
97. Dennis, M.; Duling, I. Experimental study of sideband generation in femtosecond fiber lasers. *IEEE J. Quantum Electron.* **1994**, *30*, 1469–1477. [CrossRef]
98. Weiner, A.M. Mode-Locking: Selected Advanced Topics. In *Ultrafast Optics*; John Wiley & Sons, Inc.: Hoboken, NJ, USA, 2008; pp. 316–361. [CrossRef]
99. Weiner, A.M. Ultrafast Nonlinear Optics: Third Order. In *Ultrafast Optics*; John Wiley & Sons, Inc.: Hoboken, NJ, USA, 2008; pp. 258–315. [CrossRef]
100. Fermann, M.; Bennion, I.; Sugden, K. Generation of 10 nJ picosecond pulses from a modelocked fibre laser. *Electron. Lett.* **1995**, *31*, 194–195. [CrossRef]
101. Malomed, B.A. Bound solitons in coupled nonlinear Schrödinger equations. *Phys. Rev. A* **1992**, *45*, R8321–R8323. [CrossRef] [PubMed]
102. Orekhov, I.O.; Kudelin, I.S.; Dvoretskiy, D.A.; Sazonkin, S.G.; Pnev, A.B.; Karasik, V.E.; Denisov, L.K. Propagation Features of Multibound Solitons in Optical Fiber with Anomalous Dispersion in the Telecom Range. In Proceedings of the Frontiers in Optics 2020, Washington, DC, USA, 14–17 September 2020. [CrossRef]
103. Dvoretskiy, D.A.; Sazonkin, S.G.; Kudelin, I.S.; Orekhov, I.O.; Pnev, A.B.; Karasik, V.E.; Denisov, L.K. Multibound Soliton Formation in an Erbium-Doped Ring Laser with a Highly Nonlinear Resonator. *IEEE Photonics Technol. Lett.* **2019**, *32*, 43–46. [CrossRef]
104. Nguyen, N.D.; Binh, L.N. Generation of high order multi-bound solitons and propagation in optical fibers. *Opt. Commun.* **2009**, *282*, 2394–2406. [CrossRef]
105. Chernysheva, M.; Bednyakova, A.; Al Araimi, M.; Howe, R.C.T.; Hu, G.; Hasan, T.; Gambetta, A.; Galzerano, G.; Rümmeli, M.; Rozhin, A. Double-Wall Carbon Nanotube Hybrid Mode-Locker in Tm-doped Fibre Laser: A Novel Mechanism for Robust Bound-State Solitons Generation. *Sci. Rep.* **2017**, *7*, srep44314. [CrossRef]
106. Haboucha, A.; Leblond, H.; Salhi, M.; Komarov, A.; Sanchez, F. Analysis of soliton pattern formation in passively mode-locked fiber lasers. *Phys. Rev. A* **2008**, *78*, 043806. [CrossRef]
107. Tang, D.Y.; Zhao, L.M.; Zhao, B.; Liu, A.Q. Mechanism of multisoliton formation and soliton energy quantization in passively mode-locked fiber lasers. *Phys. Rev. A* **2005**, *72*, 043816. [CrossRef]

108. Lederer, M.J.; Luther-Davies, B.; Tan, H.H.; Jagadish, C.; Akhmediev, N.N.; Soto-Crespo, J.M. Multipulse operation of a Ti:sapphire laser mode locked by an ion-implanted semiconductor saturable-absorber mirror. *J. Opt. Soc. Am. B* **1999**, *16*, 895–904. [CrossRef]
109. Dvoretskiy, D.A.; Sazonkin, S.G.; Orekhov, I.O.; Kudelin, I.S.; Pnev, A.B.; Karasik, V.E.; Denisov, L.K. Controllable Generation of Ultrashort Multi-Bound Solitons in a Mode-Locked Erbium-Doped Ring Laser with a Highly-Nonlinear Resonator. In Proceedings of the 2019 Conference on Lasers and Electro-Optics Europe and European Quantum Electronics Conference, Munich, Germany, 23–27 June 2019. [CrossRef]
110. Binh, L.N. *Optical Multi-Bound Solitons*; CRC Press: Boca Raton, FL, USA, 2015. [CrossRef]
111. Tamura, K.; Ippen, E.P.; Haus, H.A.; Nelson, L.E. 77-fs pulse generation from a stretched-pulse mode-locked all-fiber ring laser. *Opt. Lett.* **1993**, *18*, 1080–1082. [CrossRef]
112. Nelson, L.; Jones, D.; Tamura, K.; Haus, H.; Ippen, E. Ultrashort-pulse fiber ring lasers. *Appl. Phys. A* **1997**, *65*, 277–294. [CrossRef]
113. Nelson, L.E.; Fleischer, S.B.; Lenz, G.; Ippen, E.P. Efficient frequency doubling of a femtosecond fiber laser. *Opt. Lett.* **1996**, *21*, 1759–1761. [CrossRef] [PubMed]
114. Tang, D.Y.; Zhao, L.M. Generation of 47-fs pulses directly from an erbium-doped fiber laser. *Opt. Lett.* **2006**, *32*, 41–43. [CrossRef]
115. Anderson, D.; Desaix, M.; Karlsson, M.; Lisak, M.; Quiroga-Teixeiro, M.L. Wave-breaking-free pulses in nonlinear-optical fibers. *J. Opt. Soc. Am. B* **1993**, *10*, 1185–1190. [CrossRef]
116. Fermann, M.E.; Kruglov, V.I.; Thomsen, B.C.; Dudley, J.; Harvey, J.D. Self-Similar Propagation and Amplification of Parabolic Pulses in Optical Fibers. *Phys. Rev. Lett.* **2000**, *84*, 6010–6013. [CrossRef] [PubMed]
117. Buckley, J.R.; Wise, F.W.; Ilday, F.Ö.; Sosnowski, T. Femtosecond fiber lasers with pulse energies above 10 nJ. *Opt. Lett.* **2005**, 1888–1890. [CrossRef] [PubMed]
118. Peacock, A.; Kruhlak, R.; Harvey, J.; Dudley, J. Solitary pulse propagation in high gain optical fiber amplifiers with normal group velocity dispersion. *Opt. Commun.* **2002**, *206*, 171–177. [CrossRef]
119. Ortac, B.; Hideur, A.; Chédot, C.; Brunel, M.; Martel, G.; Limpert, J. Self-similar low-noise femtosecond ytterbium-doped double-clad fiber laser. *Appl. Phys. A* **2006**, *85*, 63–67. [CrossRef]
120. Ruehl, A.; Hundertmark, H.; Wandt, D.; Fallnich, C.; Kracht, D. 0.7 W all-fiber Erbium oscillator generating 64 fs wave breaking-free pulses. *Opt. Express* **2005**, *13*, 6305–6309. [CrossRef] [PubMed]
121. Proctor, B.; Westwig, E.; Wise, F. Characterization of a Kerr-lens mode-locked Ti:sapphire laser with positive group-velocity dispersion. *Opt. Lett.* **1993**, *18*, 1654–1656. [CrossRef]
122. Zhao, L.M.; Tang, D.Y.; Wu, J. Gain-guided soliton in a positive group-dispersion fiber laser. *Opt. Lett.* **2006**, *31*, 1788–1790. [CrossRef]
123. Kieu, K.; Renninger, W.H.; Chong, A.; Wise, F.W. Sub-100 fs pulses at watt-level powers from a dissipative-soliton fiber laser. *Opt. Lett.* **2009**, *34*, 593–595. [CrossRef] [PubMed]
124. Mocker, H.W.; Collins, R.J. Mode Competition and Self-Locking Effects in a *Q*-Switched Ruby Laser. *Appl. Phys. Lett.* **1965**, *7*, 270–273. [CrossRef]
125. DeMaria, A.J.; Stetser, D.A.; Heynau, H. Self Mode-Locking of Lasers with Saturable Absorbers. *Appl. Phys. Lett.* **1966**, *8*, 174–176. [CrossRef]
126. Kryukov, P.G. Ultrashort-pulse lasers. *Quantum Electron.* **2001**, *31*, 95–119. [CrossRef]
127. Hofer, M.; Fermann, M.E.; Haberl, F.; Ober, M.H.; Schmidt, A.J. Mode locking with cross-phase and self-phase modulation. *Opt. Lett.* **1991**, *16*, 502–504. [CrossRef]
128. Tamura, K.; Haus, H.; Ippen, E. Self-starting additive pulse mode-locked erbium fibre ring laser. *Electron. Lett.* **1992**, *28*, 2226–2228. [CrossRef]
129. Fermann, M.E.; Haberl, F.; Hofer, M.; Hochreiter, H. Nonlinear amplifying loop mirror. *Opt. Lett.* **1990**, *15*, 752–754. [CrossRef]
130. Richardson, D.; Laming, R.; Payne, D.; Phillips, M.; Matsas, V. 320 fs soliton generation with passively mode-locked erbium fibre laser. *Electron. Lett.* **1991**, *27*, 730–732. [CrossRef]
131. Ahmad, H.; Aidit, S.N.; Ooi, S.I.; Samion, M.Z.; Wang, S.; Wang, Y.; Sahu, J.K.; Zamzuri, A.K. 1.3 µm dissipative soliton resonance generation in Bismuth doped fiber laser. *Sci. Rep.* **2021**, *11*, 6356. [CrossRef]
132. Doran, N.J.; Wood, D. Nonlinear-optical loop mirror. *Opt. Lett.* **1988**, *13*, 56–58. [CrossRef]
133. Oh, W.-Y.; Kim, B.; Lee, H.-W. Passive mode locking of a neodymium-doped fiber laser with a nonlinear optical loop mirror. *IEEE J. Quantum Electron.* **1996**, *32*, 333–339. [CrossRef]
134. Wang, Z.; Wang, D.; Zhu, T.; Chen, J.; Chang, S. Graded index multimode fibre as saturable absorber induced by nonlinear multimodal interference for ultrafast photonics. *J. Phys. Photonics* **2020**, *3*, 012005. [CrossRef]
135. Wang, Z.; Wang, D.N.; Yang, F.; Li, L.; Zhao, C.-L.; Xu, B.; Jin, S.; Cao, S.-Y.; Fang, Z.-J. Stretched graded-index multimode optical fiber as a saturable absorber for erbium-doped fiber laser mode locking. *Opt. Lett.* **2018**, *43*, 2078–2081. [CrossRef] [PubMed]
136. Keller, U.; Miller, D.A.B.; Boyd, G.D.; Chiu, T.H.; Ferguson, J.F.; Asom, M.T. Solid-state low-loss intracavity saturable absorber for Nd:YLF lasers: An antiresonant semiconductor Fabry–Perot saturable absorber. *Opt. Lett.* **1992**, *17*, 505–507. [CrossRef]
137. Nakazawa, M.; Suzuki, K.; Kubota, H.; Kimura, Y. Self-Q-switching and mode locking in a 153-µm fiber ring laser with saturable absorption in erbium-doped fiber at 42 K. *Opt. Lett.* **1993**, *18*, 613–615. [CrossRef]
138. Set, S.; Yaguchi, H.; Tanaka, Y.; Jablonski, M. Laser Mode Locking Using a Saturable Absorber Incorporating Carbon Nanotubes. *J. Light. Technol.* **2004**, *22*, 51–56. [CrossRef]

139. Yamashita, S.; Inoue, Y.; Maruyama, S.; Murakami, Y.; Yaguchi, H.; Jablonski, M.; Set, S. Saturable absorbers incorporating carbon nanotubes directly synthesized onto substrates and fibers and their application to mode-locked fiber lasers. *Opt. Lett.* **2004**, *29*, 1581–1583. [CrossRef]
140. Yang, Q.-Q.; Liu, R.-T.; Huang, C.; Huang, Y.-F.; Gao, L.-F.; Sun, B.; Huang, Z.-P.; Zhang, L.; Hu, C.-X.; Zhang, Z.-Q.; et al. 2D bismuthene fabricated *via* acid-intercalated exfoliation showing strong nonlinear near-infrared responses for mode-locking lasers. *Nanoscale* **2018**, *10*, 21106–21115. [CrossRef]
141. Tran, V.; Soklaski, R.; Liang, Y.; Yang, L. Layer-controlled band gap and anisotropic excitons in few-layer black phosphorus. *Phys. Rev. B* **2014**, *89*, 235319. [CrossRef]
142. Koski, K.J.; Wessells, C.D.; Reed, B.W.; Cha, J.J.; Kong, D.; Cui, Y. Chemical Intercalation of Zerovalent Metals into 2D Layered Bi_2Se_3 Nanoribbons. *J. Am. Chem. Soc.* **2012**, *134*, 13773–13779. [CrossRef]
143. Zhao, J.; Xu, Z.; Zang, Y.; Gong, Y.; Zheng, X.; He, K.; Cheng, X.; Jiang, T. Thickness-dependent carrier and phonon dynamics of topological insulator Bi_2Te_3 thin films. *Opt. Express* **2017**, *25*, 14635. [CrossRef] [PubMed]
144. Jiang, T.; Yin, K.; Wang, C.; You, J.; Ouyang, H.; Miao, R.; Zhang, C.; Wei, K.; Li, H.; Chen, H.; et al. Ultrafast fiber lasers mode-locked by two-dimensional materials: Review and prospect. *Photonics Res.* **2019**, *8*, 78–90. [CrossRef]
145. Ahmad, H.; Azmy, N.F.; Reduan, S.A.; Yusoff, N.; Kadir, Z.A. Cu2Te-PVA as saturable absorber for generating Q-switched erbium-doped fiber laser. *Opt. Quantum Electron.* **2021**, *53*, 189. [CrossRef]
146. Wang, J.; Wang, X.; Lei, J.; Ma, M.; Wang, C.; Ge, Y.; Wei, Z. Recent advances in mode-locked fiber lasers based on two-dimensional materials. *Nanophotonics* **2020**, *9*, 2315–2340. [CrossRef]
147. Göbel, E.O. Ultrafast spectroscopy of semiconductors. *Festkörperprobleme* **2007**, *30*, 269–294. [CrossRef]
148. Siegner, U.; Fluck, R.; Zhang, G.; Keller, U. Ultrafast high-intensity nonlinear absorption dynamics in low-temperature grown gallium arsenide. *Appl. Phys. Lett.* **1996**, *69*, 2566–2568. [CrossRef]
149. Lederer, M.J.; Luther-Davies, B.; Tan, H.H.; Jagadish, C.; Haiml, M.; Siegner, U.; Keller, U. Nonlinear optical absorption and temporal response of arsenic- and oxygen-implanted GaAs. *Appl. Phys. Lett.* **1999**, *74*, 1993–1995. [CrossRef]
150. Lauret, J.-S.; Voisin, C.; Cassabois, G.; Delalande, C.; Roussignol, P.; Jost, O.; Capes, L. Ultrafast Carrier Dynamics in Single-Wall Carbon Nanotubes. *Phys. Rev. Lett.* **2003**, *90*, 057404. [CrossRef]
151. Bale, B.G.; Okhitnikov, O.G.; Turitsyn, S.K. Modeling and Technologies of Ultrafast Fiber Lasers. In *Fiber Lasers*; John Wiley & Sons, Ltd.: Hoboken, NJ, USA, 2012; pp. 135–175. [CrossRef]
152. Byun, H.; Pudo, D.; Chen, J.; Ippen, E.P.; Kärtner, F.X. High-repetition-rate, 491 MHz, femtosecond fiber laser with low timing jitter. *Opt. Lett.* **2008**, *33*, 2221–2223. [CrossRef]
153. Chen, J.; Sickler, J.W.; Byun, H.; Ippen, E.P.; Jiang, S.; Kärtner, F.X. Fundamentally Mode-locked 3 GHz Femtosecond Erbium Fiber Laser. In *Ultrafast Phenomena XVI*; Corkum, P., Silvestri, S., Nelson, K.A., Riedle, E., Schoenlein, R.W., Eds.; Springer: Berlin/Heidelberg, Germany, 2009; Volume 92, pp. 732–734. [CrossRef]
154. Guina, M.; Xiang, N.; Okhotnikov, O. Stretched-pulse fiber lasers based on semiconductor saturable absorbers. *Appl. Phys. A* **2002**, *74*, s193–s200. [CrossRef]
155. Chen, Y.-C.; Raravikar, N.R.; Schadler, L.S.; Ajayan, P.M.; Zhao, Y.-P.; Lu, T.-M.; Wang, G.-C.; Zhang, X.-C. Ultrafast optical switching properties of single-wall carbon nanotube polymer composites at 1.55 µm. *Appl. Phys. Lett.* **2002**, *81*, 975–977. [CrossRef]
156. Huang, L.; Zhang, Y.; Liu, X. Dynamics of carbon nanotube-based mode-locking fiber lasers. *Nanophotonics* **2020**, *9*, 2731–2761. [CrossRef]
157. Set, S.; Yaguchi, H.; Tanaka, Y.; Jablonski, M.; Sakakibara, Y.; Rozhin, A.; Tokumoto, M.; Kataura, H.; Achiba, Y.; Kikuchi, K. Mode-locked fiber lasers based on a saturable absorber incorporating carbon nanotubes. In Proceedings of the Optical Fiber Communications Conference, Atlanta, GA, USA, 28 March 2003; Volume 3, p. PD44-P1-3. [CrossRef]
158. Hong, S.; Myung, S. Nanotube Electronics: A flexible approach to mobility. *Nat. Nanotechnol.* **2007**, *2*, 207–208. [CrossRef] [PubMed]
159. Pop, E.; Mann, D.; Wang, Q.; Goodson, K.; Dai, H. Thermal Conductance of an Individual Single-Wall Carbon Nanotube above Room Temperature. *Nano Lett.* **2006**, *6*, 96–100. [CrossRef]
160. Meo, M.; Rossi, M. Prediction of Young's modulus of single wall carbon nanotubes by molecular-mechanics based finite element modelling. *Compos. Sci. Technol.* **2006**, *66*, 1597–1605. [CrossRef]
161. Set, S.; Yaguchi, H.; Tanaka, Y.; Jablonski, M. Ultrafast Fiber Pulsed Lasers Incorporating Carbon Nanotubes. *IEEE J. Sel. Top. Quantum Electron.* **2004**, *10*, 137–146. [CrossRef]
162. Tatsuura, S.; Furuki, M.; Sato, Y.; Iwasa, I.; Tian, M.; Mitsu, H. Semiconductor Carbon Nanotubes as Ultrafast Switching Materials for Optical Telecommunications. *Adv. Mater.* **2003**, *15*, 534–537. [CrossRef]
163. Cho, W.B.; Yim, J.H.; Choi, S.Y.; Lee, S.; Schmidt, A.; Steinmeyer, G.; Griebner, U.; Petrov, V.; Yeom, D.-I.; Kim, K.; et al. Boosting the Non Linear Optical Response of Carbon Nanotube Saturable Absorbers for Broadband Mode-Locking of Bulk Lasers. *Adv. Funct. Mater.* **2010**, *20*, 1937–1943. [CrossRef]
164. Martinez, A.; Sun, Z. Nanotube and graphene saturable absorbers for fibre lasers. *Nat. Photonics* **2013**, *7*, 842–845. [CrossRef]
165. Mirza, S.; Rahman, S.; Sarkar, A.; Rayfield, G. Carbon Nanotubes for Optical Power Limiting Applications. In *Nanoscale Photonics and Optoelectronics*; Wang, Z.M., Neogi, A., Eds.; Springer: New York, NY, USA, 2010; Volume 9, pp. 101–129. [CrossRef]

166. Dvoretskiy, D.A.; Sazonkin, S.G.; Orekhov, I.O.; Kudelin, I.S.; Pnev, A.B.; Karasik, V.E.; Denisov, L.K.; Davydov, V.A. Low-saturation-energy Ultrafast Saturable Absorption of High-density Well-aligned Single-walled Carbon Nanotubes. In *Applications of Lasers for Sensing and Free Space Communications*; Optical Society of America: Vienna, Austria, 2019; p. JW2A-2. [CrossRef]
167. Ivanov, V.; Fonseca, A.; Nagy, J.B.; Lucas, A.; Lambin, P.; Bernaerts, D.; Zhang, X.B. Catalytic production and purification of nanotubules having fullerene-scale diameters. *Carbon* **1995**, *33*, 1727–1738. [CrossRef]
168. Hasan, T.; Sun, Z.; Wang, F.; Bonaccorso, F.; Tan, P.H.; Rozhin, A.G.; Ferrari, A.C. Nanotube-Polymer Composites for Ultrafast Photonics. *Adv. Mater.* **2009**, *21*, 3874–3899. [CrossRef]
169. Baek, I.H.; Lee, H.W.; Bae, S.; Hong, B.H.; Ahn, Y.H.; Yeom, D.-I.; Rotermund, F. Efficient Mode-Locking of Sub-70-fs Ti:Sapphire Laser by Graphene Saturable Absorber. *Appl. Phys. Express* **2012**, *5*, 032701. [CrossRef]
170. Popa, D.; Sun, Z.; Hasan, T.; Cho, W.B.; Wang, F.; Torrisi, F.; Ferrari, A.C. 74-fs nanotube-mode-locked fiber laser. *Appl. Phys. Lett.* **2012**, *101*, 153107. [CrossRef]
171. Yu, Z.; Wang, Y.; Zhang, X.; Dong, X.; Tian, J.; Song, Y. A 66 fs highly stable single wall carbon nanotube mode locked fiber laser. *Laser Phys.* **2013**, *24*, 015105. [CrossRef]
172. Kim, C.; Bae, S.; Kieu, K.; Kim, J. Sub-femtosecond timing jitter, all-fiber, CNT-mode-locked Er-laser at telecom wavelength. *Opt. Express* **2013**, *21*, 26533–26541. [CrossRef]
173. Lazarev, V.; Krylov, A.; Dvoretskiy, D.; Sazonkin, S.; Pnev, A.; Leonov, S.; Shelestov, D.; Tarabrin, M.; Karasik, V.; Kireev, A.; et al. Stable Similariton Generation in an All-Fiber Hybrid Mode-Locked Ring Laser for Frequency Metrology. *IEEE Trans. Ultrason. Ferroelectr. Freq. Control* **2016**, *63*, 1028–1033. [CrossRef]
174. Dvoretskiy, D.A.; Lazarev, V.A.; Voropaev, V.S.; Rodnova, Z.N.; Sazonkin, S.G.; Leonov, S.O.; Pnev, A.B.; Karasik, V.E.; Krylov, A.A. High-energy, sub-100 fs, all-fiber stretched-pulse mode-locked Er-doped ring laser with a highly-nonlinear resonator. *Opt. Express* **2015**, *23*, 33295–33300. [CrossRef]
175. Dvoretskiy, D.; Sazonkin, S.G.; Voropaev, V.S.; Leonov, S.O.; Pnev, A.B.; Karasik, V.E.; Krylov, A.A.; Obraztsova, E.D. Dispersion-managed soliton generation in the hybrid mode-locked erbium-doped all-fiber ring laser. In Proceedings of the 2016 International Conference Laser Optics, LO 2016, St. Petersburg, Russia, 27 June–1 July 2016. [CrossRef]
176. Fermann, M.E. Nonlinear polarization evolution in passively modelocked fiber lasers. In *Compact Sources of Ultrashort Pulses*; Irl, I.I.I., Duling, N., Eds.; Cambridge University Press: Cambridge, UK, 1995; pp. 179–207.
177. Buckley, J. *High-Energy Ultrafast Ytterbium Fiber Lasers*; Cornell University: Ithaca, NY, USA, 2006.
178. Maker, P.D.; Terhune, R.W. Study of Optical Effects Due to an Induced Polarization Third Order in the Electric Field Strength. *Phys. Rev.* **1965**, *137*, A801–A818. [CrossRef]
179. Dahlström, L. Mode-locking of high power lasers by a combination of intensity and time dependent Q-switching. *Opt. Commun.* **1973**, *7*, 89–92. [CrossRef]
180. Ma, D.; Cai, Y.; Zhou, C.; Zong, W.; Chen, L.; Zhang, Z. 374 fs pulse generation in an Er:fiber laser at a 225 MHz repetition rate. *Opt. Lett.* **2010**, *35*, 2858–2860. [CrossRef]
181. Fermann, M.; Hofer, M. Mode-Locked Fiber Lasers. In *Rare-Earth-Doped Fiber Lasers and Amplifiers*; Digonnet, M.J.F., Ed.; Marcel Dekker, Inc.: New York, NY, USA, 2001; p. 418. [CrossRef]
182. Fermann, M.E.; Yang, L.-M.; Stock, M.L.; Andrejco, M.J. Environmentally stable Kerr-type mode-locked erbium fiber laser producing 360-fs pulses. *Opt. Lett.* **1994**, *19*, 43–45. [CrossRef] [PubMed]
183. Mortimore, D. Fiber loop reflectors. *J. Light. Technol.* **1988**, *6*, 1217–1224. [CrossRef]
184. Hui, R. Chapter 6—Passive optical components. In *Introduction to Fiber-Optic Communications*; Hui, R., Ed.; Academic Press: Cambridge, MA, USA, 2020; pp. 209–297. [CrossRef]
185. Zhao, L.M.; Bartnik, A.C.; Tai, Q.Q.; Wise, F.W. Generation of 8 nJ pulses from a dissipative-soliton fiber laser with a nonlinear optical loop mirror. *Opt. Lett.* **2013**, *38*, 1942–1944. [CrossRef] [PubMed]
186. Gong, Q.; Zhang, H.; Deng, D.; Zu, J. Dissipative Soliton Resonance in an All-Polarization Maintaining Fiber Laser With a Nonlinear Amplifying Loop Mirror. *IEEE Photonics J.* **2020**, *12*, 1502708. [CrossRef]
187. Nakazawa, M.; Yoshida, E.; Kimura, Y. Generation of 98 fs optical pulses directly from an erbium-doped fibre ring laser at 1.57 μm. *Electron. Lett.* **1993**, *29*, 63–65. [CrossRef]
188. Kovalev, A.V.; Viktorov, E.A.; Vladimirov, A.; Rebrova, N.; Huyet, G. Theoretical study of mode-locked lasers with nonlinear loop mirrors. In *Semiconductor Lasers and Laser Dynamics VIII*; SPIE: Bellingham, WA, USA, 2018; Volume 10682, p. 1068226. [CrossRef]
189. Orekhov, I.O.; Sazonkin, S.G.; Bugai, K.E.; Dvoretskiy, D.A.; Shelestov, D.A.; Koshelev, K.V.; Khan, R.I.; Karasik, V.E.; Denisov, L.K.; Davydov, V.A. Mode-locking features in a sub-200-fs erbium-doped all-fiber laser based on high-density well-aligned single-walled carbon nanotubes. In *Nonlinear Optics and Applications XII*; SPIE: Bellingham, WA, USA, 2021; Volume 11770. [CrossRef]
190. Li, X.; Zou, W.; Chen, J. 419 fs hybridly mode-locked Er-doped fiber laser at 212 MHz repetition rate. *Opt. Lett.* **2014**, *39*, 1553–1556. [CrossRef] [PubMed]
191. Liu, Y.; Zhang, J.-G.; Chen, G.; Zhao, W.; Bai, J. Low-timing-jitter, stretched-pulse passively mode-locked fiber laser with tunable repetition rate and high operation stability. *J. Opt.* **2010**, *12*, 095204. [CrossRef]
192. Xiao, L.; Wang, T.; Ma, W.; Zhao, R. Hybrid Mode-Locked 2μm Fiber Laser Based on Nonlinear Polarization Rotation and Semiconductor Saturable Absorber Mirror. In Proceedings of the 2021 13th International Conference on Advanced Infocomm Technology, ICAIT 2021, Yanji, China, 15–18 October 2021; pp. 38–41. [CrossRef]

193. Xu, B.; Martinez, A.; Set, S.; Goh, C.S.; Yamashita, S. A net normal dispersion all-fiber laser using a hybrid mode-locking mechanism. *Laser Phys. Lett.* **2013**, *11*, 25101. [CrossRef]
194. Ilday, F.; Wise, F.W.; Sosnowski, T. High-energy femtosecond stretched-pulse fiber laser with a nonlinear optical loop mirror. *Opt. Lett.* **2002**, *27*, 1531–1533. [CrossRef]
195. Kim, S.; Kim, Y.; Park, J.; Han, S.; Park, S.; Kim, Y.-J.; Kim, S.-W. Hybrid mode-locked Er-doped fiber femtosecond oscillator with 156 mW output power. *Opt. Express* **2012**, *20*, 15054–15060. [CrossRef]